Department of Electrical and Computer Systems Engineering

Technical Report
MECSE-10-2005

Apodized Fiber Bragg Gratings: Novel Fabrication, Nonlinear Chirp, Profile Reconstruction and Synthesis Optimisation

LN Binh, RT Zheng and N.Q.Ngo

MONASH UNIVERSITY

APODIZED FIBER BRAGG GRATINGS:

NOVEL FABRICATION, NONLINEAR CHIRP, PROFILE RECONSTRUCTION AND SYNTHESIS OPTIMISATION[1]

LN Binh*, RT Zheng# and N.Q.Ngo#

* Laboratory for Optical Communications and Applied Photonics, Department of Electrical and Computer Systems Engineering, Monash University, Clayton Victoria Australia

Photonic Research Centre, School of Electrical and Electronic Engineering, Nanyang Technological University, Singapore

ABSTRACT

This report consists of four principal sections for the fabrication of FBGs under pre-stretched conditions to produce continuous linear and nonlinear chirped (apodized) structures and optimization methods for the reconstruction of the modulation index profile of the gratings, and an optimum search algorithm for grating syntheses with targeted group delay properties.

*First, we present the design, fabrication and testing of **the piece-wise stepped-chirp fiber Bragg gratings (FBGs)** with arbitrary group delay responses using a uniform phase mask **under pre-stretched condition.** The method involves writing a series of sub-gratings on a pre-stretched fiber whose length is varied during the UV exposure process. Two motorized stages are employed to control the length of the pre-stretched fiber in order to adjust the grating pitch at each writing step to achieve piece-wise stepped chirping of the FBG. Because the fiber is moved relatively to the phase mask, an apodized index modulation profile of the FBG can be obtained by fiber dithering. To demonstrate the effectiveness of the method to produce FBGs with arbitrary group delay responses, a linear-chirp non-apodized FBG and a quadratic-chirp apodized FBG were fabricated, and their experimental results agree well with the analytical predictions.*

*Secondly, a **novel fabrication method to generate continuous nonlinear chirp fiber Bragg gratings** using a uniform phase mask is described when the fiber is under pre-stretched condition. A motorized stage controls the stretched length while scanning of the UV beam. Nonlinear group delay has been observed and a good agreement with the analytical results is obtained. This indicates that the FBG can be used as an effective tuneable dispersion compensator.*

*Thirdly, a **new and simple method is report for reconstructing the refractive-index modulation** of a symmetric FBG from its reflectance spectrum that is the*

---

[1] Some parts of the report have been the subjects of published articles [47-50].

*phase information is not needed. The reconstruction method uses an FBG model based on some known properties of the fabricated FBG including the grating length, the number of sub-gratings, and the grating period. An optimization technique, namely, the Quasi-Newton method is applied to find the local parameter values of the FBG. The **reconstruction of FBG, to our knowledge, for the first time, is experimentally realized by an optimization technique**. Comparing with other reconstruction methods, the proposed method is much simpler as it only requires the reflectance spectrum of the fabricated FBG for optimization.*

*Finally, a **novel staged continuous Tabu search (SCTS) algorithm** is proposed for solving global optimization multi-variable problems of multi-minima functions. The proposed method comprises three stages with different neighbor-search strategies.. The method searches for the global optimum thoroughly and efficiently over the solution space. The effectiveness of the proposed SCTS algorithm is evaluated using a set of benchmark multimodal functions whose global and local minima are known. Numerical test results obtained indicate that the proposed method is more efficient than the genetic algorithm. The method is then applied to the design optimization and automation for the fabrication of apodized FBGs for dispersion compensation in optical transmission systems.. Compared with two other well-known algorithms, namely, genetic algorithm (GA) and simulated annealing (SA), **the proposed method performs much more efficient, in computing speed and convergence, for the optimization of the FBG design***.

TABLE OF CONTENTS

TABLE OF FIGURES

1   PREAMBLE

Fibre Bragg gratings are the most commonly used passive photonic devices in the last decades. The uniformed and chirped gratings have been extensively investigated. However they are normally fabricated by exposing the photorefractive sensitive fibre under relaxed conditions. This report describes novel techniques for fabrication of FBGs with arbitrary group delay responses when the fiber is under extension or compression, i.e. in-situ pre-stretching. The group delay can be nonlinear if the bare fiber is continuously stressed during the grating UV writing. Piece-wise stepped chirp gratings are also fabricated. An optimisation method is developed to reconstruct the inde profile of the gratings and applied as a control mechanism for fabrication of FBG with some specified group delay responses.

The report is organised in a number of sub-sections. Section 2 describes the fabrication and simplified design for FBGs with step chirp characteristics when the fibre is under pre-stretched conditions. Section 3 extends further with the methodology for producing non-linear group delay in chirped FBG with the principal objective for used as a dispersion compensator in long-haul optical networks. Section 4 outlines the reconstruction technique for the determination of the modulation of the refractive index profile distributed along the UV written area. Section 5 then describes search algorithm for syntheses of the FBG profile so as to serve as an automatic control of the FBG fabrication system.

Details of the works and motivation for developing these apodized FBGs and method of reconstruction are given in the introductory remarks of the sub-sections. Concluding remarks are also given at the end of these sub-sections.

2   PRE-STRETCHED CHIRPED FBGS

Chirped FBGs (CFBG) are gratings with their Bragg wavelengths varying linearly or nonlinearly along the grating length. CFBGs have been widely used for dispersion compensation, pulse multiplication and pulse compression [1-3]. To fabricate CFBGs to tailor for different applications, several techniques have been developed. One method involves the use of a chirped phase mask. However, a chirped phase mask is expensive, and the fabricated gratings always exhibit a fixed group delay characteristics. To overcome this drawback, considerable attempts have been made to fabricate chirped gratings using a less expensive uniform phase mask. These methods are dual-scanning technique [4], shifting the Bragg wavelength by the addition of a converging lens before the mask [5], and moving fiber/phase mask-scanning beam technique [6]. A technique for fabrication of long gratings with complex profiles was developed in [7]. The idea was to expose a large number of small partially overlapping sub-gratings in sequence by UV pulses. Each sub-grating contained a

few hundred periods or less. Thus the advanced properties such as chirp, phase shifts, and apodization were introduced by adjusting the phase offset and pitch of the sub-gratings. Pertermann and his colleagues further improved the method by using continuous wave (CW) UV source and a sawtooth movement of the interference pattern [8]. With this method, the grating period was varied with the interferometric setup. This method requires high position accuracy and they use an interferometric system to monitor the translation stage.

The design of stepped-chirp fiber Bragg gratings has been discussed by Kashyap [9], By using a stepped chirp phase mask, the stepped chirp FBG can be fabricated [10]. Reference [11] presents a stretching and writing technique to fabricate such stepped chirp FBG. In this method, the Bragg wavelength along the grating length can be adjusted by controlling the strain of the fiber during UV exposure compared with method presented in [8], which controlling the interferometric setup. Because the interferometer to inscribe the grating is formed by a uniform phase mask, the exposure process is comparable stable. However, Ref. [11] has not studied the relationship between the group delay response of FBG and the corresponding fabrication parameters, thus tailoring chirped gratings with arbitrary group delay responses is still a challenging problem with this method. Furthermore, the fiber is stretched on one side during writing process in the method presented in [11], so that the fabrication process might take a big phase error to the fabricated grating.

We inscribe the step-chirped FBG with an arbitrary group delay response using a uniform phase mask in a pre-stretched fiber. Two motorized stages are employed to stretch the length of the fiber during UV exposure to obtain a desired group delay response. In order to control the phase of the grating continuously, hence a constant group delay response, the moved lengths of two motorized stages are dynamically assigned. The fiber can be dithered by two stages during an exposure process to realize an apodized grating profile. To obtain a constant distribution of strain along the pre-stretched fiber, the coating of the fiber is stripped off before the UV writing.

The main improvement of the proposed method over the method presented in [11] is that the proposed method uses two stages to stretch the fiber to minimize the phase error. Furthermore, the coating of the fiber is stripped off while the coating was left in the method presented in [11]. Because the coatings will decrease the UV exposure efficiency, our method can produce stronger gratings than those reported in [11]. In this section, a linearly chirped FBG and a nonlinearly-chirped FBG are fabricated using the proposed method. The measured reflective spectra and the group delay responses of the linearly chirped FBG and the nonlinearly chirped FBG are consistent with our analytical predictions.

2.1   Fiber Stretching FBG Fabrication and Analytical Techniques

Figure 1 shows the schematic diagram of the setup used for fabricating the FBGs with arbitrary group delay responses. The UV beam from a frequency-doubled Argon laser is folded by a mirror mounted on a motorized translation stage and focused using a cylindrical lens onto the pre-stretched fiber through the phase mask. The UV beam scans along the pre-stretched fiber. The scanning velocity is controlled by a motorized translation stage. The fiber is clamped by two motorized stages (i.e. Stage A and Stage B). The mounted fiber is then pre-stretched before the UV exposure so that the fiber length can either be increased or decreased by stretching or releasing the fiber respectively. The plastic coating of the fiber might reduce the exposure efficiency and hence reducing the grating depth. The gratings used for dispersion compensation tend to be strong so the gratings are often inscribed with the coatings stripped off. To obtain a constant distribution of the in-fiber strain along the fiber length, the plastic coating of a segment of the fiber between the two holders is removed including the segment without the inscribed grating. The coating in the segment in the holders is not stripped off to avoid slippage.

The photosensitivity of the fiber could be altered with different in-fiber strain. However, the change of the in-fiber strain is quite small, thus the effect on the photosensitivity of the in-fiber strain can be ignored in our experiments. The original distance between the two stages is L_1 during the UV scanning of the first sub-grating. Before the second sub-grating is written, both ends of the fiber (with length L_1) are stretched. The fiber length now becomes $L_2 = L_1 + x_1$, with x_1 as the stretching amount at both fiber ends, and $L_2 > L_1$ for $x_1 > 0$ (i.e. stretching the fiber) or $L_2 < L_1$ for $x_1 < 0$ (i.e. releasing the fiber). That means, the stretched length $x_1 = x_A^1 + x_B^1$ is the amount of movement of Stage A and Stage B, where x_A^1 and x_B^1 are the distances moved by Stage A and Stage B, respectively (see **Figure 1**). And l_1 is the distance between Stage A and the position between the first sub-grating and the second sub-grating. After the fiber is stretched (or elongated), it is moved relatively to the phase mask. As a result, a phase shift could be inserted between two neighboring sub-gratings.
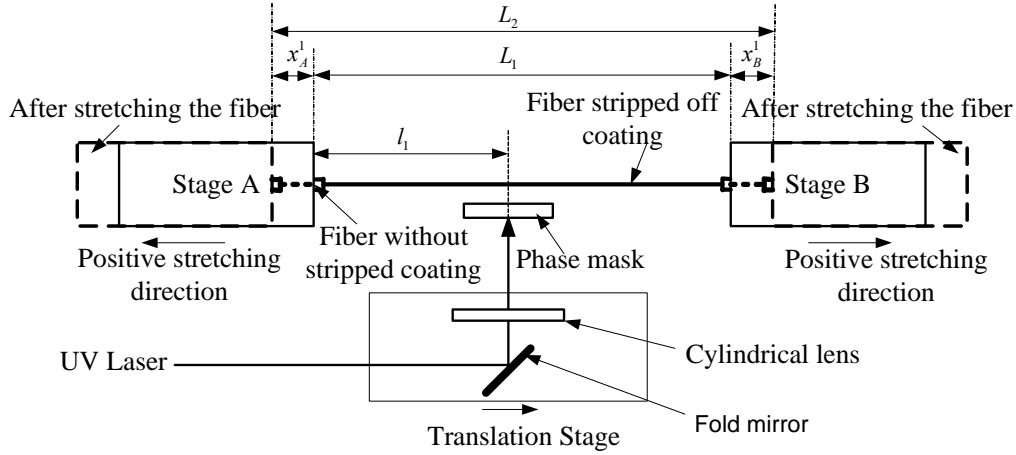
Figure 1 *Schematic diagram of the system setup for fabricating the chirped FBG with arbitrary group delay responses.*

When the moving distances of Stage A and Stage B follow the following relationships

$$x_A^1 = \frac{x_1 l_1}{L_1} \text{ and } x_B^1 = x_1 - x_A^1 = \frac{x_1(L_1 - l_1)}{L_1} \tag{1}$$

then the phase of the grating can be kept continuous (i.e. no phase shift is inserted between neighboring sub-gratings). After stretching the fiber, the grating period of the first sub-grating are elongated (i.e. $L_2 > L_1$). Thus the difference in the grating periods between the first sub-grating and the second sub-grating can be described by

$$\Delta\Lambda_1 = \frac{x_1}{2L_1}\Lambda_p \tag{2}$$

where Λ_p is the period of the phase mask. The index modulation of the grating will be averaged when the UV beam illuminate the fiber in moving. To avoid it, the UV beam will be shielded when the fiber is stretched. Thus a chirped grating fabricated with N steps can be formed after fabricating a number of consecutive sub-gratings with a serious of stretched lengths between any two neighboring sub-gratings as described by $\vec{X} = \{x_1, x_2, \ldots, x_{N-1}\}$. The variation of the fiber length during stretching is given by $\vec{L} = \{L_1, L_2, \ldots, L_N\}$, where L_i is the fiber length when inscribing the ith sub-grating. Assuming that the average fiber length is given by $L_{avg} = \frac{L_1 + L_2 + \cdots + L_N}{N}$ and using the fact that $L_i >> x_i$, we have $L_1 \approx L_2 \approx \cdots \approx L_{avg}$. The longitudinal position of the ith sub-grating along the fiber length is z_i

$= i \times \Delta z$, where $i = 1, 2, …, N$, is the section number and Δz is the length of each sub-grating. Thus the Bragg wavelength at position z_i can be approximately given as

$$\lambda(z_i) = \lambda_1 + 2n_{eff} \sum_{k=1}^{i} \Delta\Lambda_k = \lambda_1 + \frac{n_{eff}\Lambda_p}{L_{avg}} \sum_{j=1}^{\frac{z_i}{\Delta z}-1} \overrightarrow{X}(j) \tag{3}$$

where n_{eff} is the effective index of the grating, and λ_1 is the Bragg wavelength of the first sub-grating which can be determined by the initial strain applied to the fiber. Thus the grating fabricated by the method will have a stepped-chirp grating period as the same characters as presented in [9] [10]. ***Figure 2*** shows the schematic diagram of such kind of stepped-chirp grating.
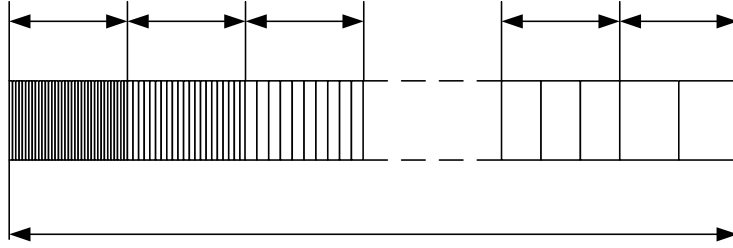
Figure 2 *Schematic of a step-chirped grating, showing N equal sections of δl each with a different period [10].*

The time delay of the grating can be calculated by computing the change in phase as a function of wavelength λ_i [9] [12] as given by

$$\tau(\lambda_i) = \frac{\partial\phi}{\partial\omega} = -\frac{\lambda_i^2}{2\pi c}\frac{\partial\phi}{\partial\lambda} \tag{4}$$

For chirped grating, the phase variation along the grating length z can be obtained by [13]

$$\frac{1}{2}\frac{\partial\phi}{\partial z} = -\frac{4\pi n_{eff} z}{\lambda^2}\frac{d\lambda}{dz} \tag{5}$$

substituting (5) into (4) gives

$$\tau(\lambda_i) = 2n_{eff} z / c \tag{6}$$

where c is the speed of light in vacuum. It should be noted that the distance between Stage A and the exposure position, that is $\vec{l} = \{l_1, l_2, …, l_{N-1}$ where $l_{N-1} > l_2 > l_1)$, becomes longer during

the UV writing process. The stretched lengths, $\overrightarrow{x_A} = \left\{x_A^1, x_A^2, \cdots, x_A^{N-1}\right\}$ and $\overrightarrow{x_B} = \left\{x_B^1, x_B^2, \cdots, x_B^{N-1}\right\}$ must be dynamically set according to (1) to obtain a stepped-chirp grating with continuous phase distribution.

2.2 Spectra and Delay Responses

In the experiment, we inscribed the grating onto a Ge:doped fiber (PMS 50 from Stock Yale). The period of the phase mask is 1070 nm. The power of the UV laser is 50 mW. The translation stage we used is Newport PM500-LW (the accuracy is $0.2\mu m$) and the two stages used for stretch the fiber are from Newport either, which have the accuracy of $0.05\mu m$.

First, a unapodized linearly chirped grating is fabricated. To obtain a linearly chirped grating, the different stretched lengths are set to be the same (i.e. $x_1 = x_2 = \ldots = x_{N-1} = x_c$, where x_c is a constant value). For a linearly chirped FBG, the corresponding set of Bragg wavelengths of the sub-gratings along the stretched fiber can be derived from (3) as

$$\lambda(z_i) = \lambda_1 + \frac{n_{eff}\Lambda_p x_c}{L_{avg}} \times (\frac{z_i}{\Delta z} - 1) \tag{7}$$

Thus the group delay $\tau(\lambda)$ of a linearly chirped FBG relates to this set of Bragg wavelengths as

$$\tau(\lambda) = \frac{2\Delta z \cdot L_{avg}}{\Lambda_p x_c c}(\lambda - \lambda_1) + \frac{2n_{eff}\Delta z}{c} \tag{8}$$

The dispersion factor of a linearly chirped FBG can be derived from (8) as

$$D = \frac{d\tau}{d\lambda} = \frac{2\Delta z L_{avg}}{\Lambda_p x_c c} \tag{9}$$

The velocity of the translation stage is 0.01 mm/s. The initial length of the pre-stretched fiber, L_1, between Stage A and Stage B is $L_{avg} = 193\,mm$. The number of sub-gratings is 50 and the total length of the FBG is 25 mm. Thus the length of the sub-grating is $\Delta z = 25\,mm/50 = 0.5\,mm$. The stretched length profile is set as $\overrightarrow{X} = \{5, 5, \ldots, 5\}\,\mu m$ and thus $x_c = 5\,\mu m$. Substituting these parameter values into (8) gives the dispersion of the FBG of 120.25 ps/nm.

Figure 3 shows the measured reflective spectrum and group delay response of the fabricated linearly chirped FBG. The in-band dispersion is ~123.9 ps/nm and is quite close to the theoretical value of 120.25 ps/nm. **Figure 3** shows the deviation of the linear portion of the

group delay. However, there are some ripples in the reflective spectrum shown in Fig. 2, with the largest ripple of ~10 dB at a wavelength of 1552.7 nm. Such ripples are caused by some positioning errors, due to the precision control of $\vec{x}_A$ and $\vec{x}_B$, and hence errors in controlling the grating phase.
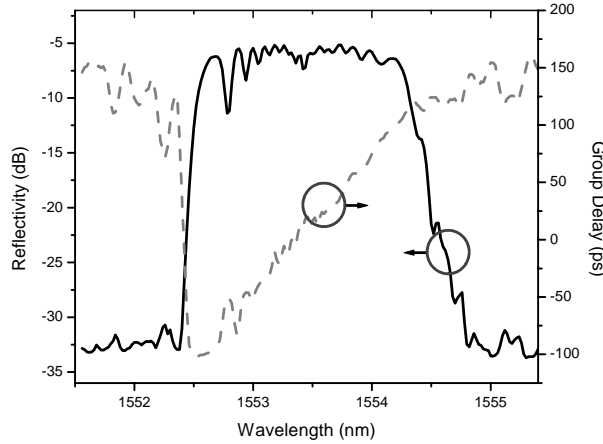
Figure 3 Measured reflective spectrum and group delay response of a linearly chirped FBG.

Second, we the apply the same developed technique to fabricate apodized quadratic-chirp FBGs. To produce a quadratic chirp profile, the stretched lengths are set as $\overrightarrow{X}(i) = x_1 - k(i-1)$, where i = 1, 2,..., N–1, and k is a constant value. Using (3) and (4), we can derive the group delay as a function of the Bragg wavelength of a quadratic chirp FBG as

$$\tau(\lambda) = -\frac{2n_{eff}\Delta z(x_1 + k/2)}{k \cdot c}\left[1 - \frac{2kL_{avg}}{n_{eff}\Lambda_p(x_1 + k/2)^2}(\lambda - \lambda_1)\right]^{1/2} + C \tag{10}$$

where C is a constant. If (10) is expanded by a Taylor series, we can obtain

$$\tau(\lambda) = \tau(\lambda_1) + \frac{2\Delta z L_{avg}}{c\Lambda_p(x_1 + k/2)}(\lambda - \lambda_1) + \frac{1}{2!}\cdot\left(\frac{kL_{avg}^2}{2n_{eff}\Lambda_p^2 c(x_1 + k/2)^3}\right)\cdot(\lambda - \lambda_1)^2 + ... \tag{11}$$

The velocity of the translation stage is 5 μm/s. The initial length of the pre-stretched fiber, L_1, between Stage A and Stage B is $L_{avg} = 193\,\text{mm}$. The number of sub-gratings is 100, the total length of the FBG is 50 mm and hence $\Delta z = 50\,\text{mm}/100 = 0.5\,\text{mm}$. The stretched length of the ith section was set as $x(i) = x_1 - 0.029(i-1)$ μm where i = 1, 2,..., N–1. Substituting these parameters into (10) gives the linear coefficient of the time delay of 164.1 ps/nm and the quadratic coefficient (or dispersion slope) of 21.3 ps/nm^2.

Figure 4 shows the measured reflectivity spectrum and the group delay response of the quadratic-chirp FBG. **Figure 5** shows the quadratic part of the measured in-band group delay response that means the linear portion of the GD has been eliminated. The estimated linear coefficient is 158.9 ps/nm and the quadratic coefficient is 19.7 ps/nm^2.

As described above, the large ripples in the reflective spectra of both the linearly chirped FBG and the quadratic chirp FBG are probably due to the positioning errors due to precision of the control of $\vec{x}_A$ and $\vec{x}_B$, hence the errors in controlling the phases of the two FBGs. This problem could be overcome by using more precise controllers such as PZT controllers instead of the motorized stages (i.e. Stage A and Stage B).

The main limitation of the presented method is the bandwidth of the fabricated grating. It is mainly determined by the photosensitivity of fiber core material. Ref. [13] has reported that gratings fabricated onto a polymeric core have a tunable spectral range of about 20 nm. However, if an increase of the bandwidth of the fabricated grating is required then the strain of the fiber is higher during fabrication. As a result, the fabrication process demands a higher accuracy of the positioning devices. **Figure 6** shows the deviation of the linear time delay of the measured in-band group delay response of a quadratic-chirp FBG. The estimated dispersion and dispersion slope are 158.9 ps/nm and 19.7 ps/nm^2 respectively.
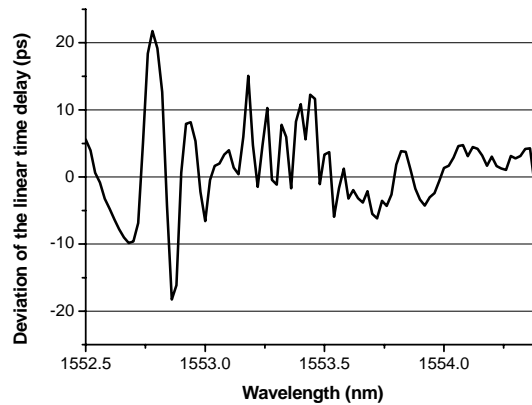
Figure 4 Deviation of the linear time delay of the measured in-band group delay response. The estimated dispersion factor is 123.9 ps/nm.
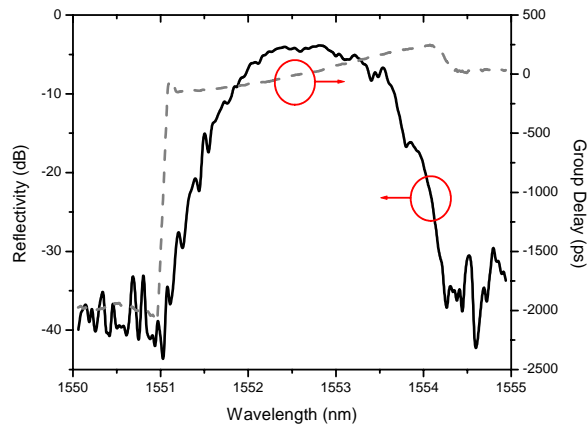
Figure 5 Measured reflective spectrum and group delay response of a quadratic chirp FBG.
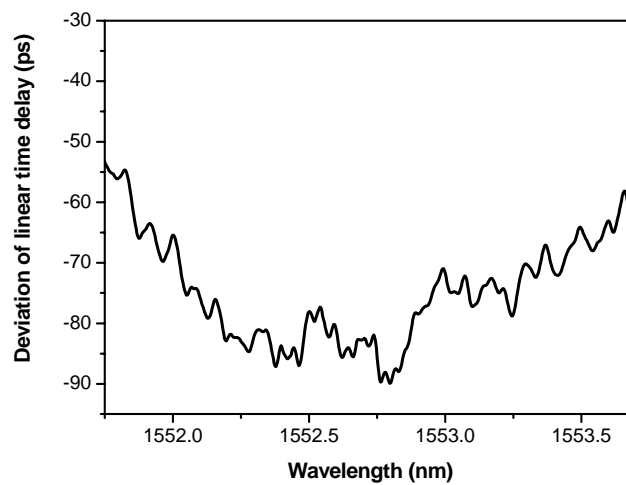
Figure 6 Deviation of the linear time delay of the measured in-band group delay response of a quadratic chirp FBG. The estimated dispersion and dispersion slope are 158.9 ps/nm and 19.7 ps/nm^2 respectively.

2.3 Remarks

In this section the design and fabrication of the piece-wise stepped-chirp fiber Bragg gratings (FBGs) are given. They can be written using a uniform phase mask while the bare fiber is under pre-stretching to produce FBGs with arbitrary group delay responses. The group delay spectral response can be arbitrarily generated by continuously varying the tension of the fiber during UV exposure to introduce phase shifts into the grating structure to realize apodization

of the index modulation profile. A non-apodized linearly chirped FBG and an apodized quadratic chirp FBG have been fabricated using this method. The measured group delay responses of these two types of FBGs show a good agreement with analytical predictions.

3   ASYMMETRIC CHIRPED FBGs

This section reports a novel fabrication method to generate continuous chirp FBGs using a uniform phase mask. The fiber is in a pre-stretched state as demonstrated in the previous section but with a motorized stage continuously controling the stretched length while scanning of the UV beam.   Nonlinear group delay has been achieved in good agreement with analytical results.

The accumulated dispersion and nonlinearities are two of the most troublesome issues in fiber transmission operating at speed higher than 10 Gb/s. Further optical communication systems operating at 40 Gb/s advanced modulation formats such as the vestigial single sideband (VSB) RZ or NRZ requires optical filters that could reject half of the unwanted band [14] with high rejection ratio on one side and tolerable roll-off band on the other.

Nonlinearly chirped fiber Bragg gratings (NCFBGs) have been recognized to be one of the most attractive solutions [15,16]. However, due to the difficulty in producing nonlinear chirped phase mask, considerable efforts have been conducted to fabricate NCFBGs using a uniform phase mask, such as applying temperature gradient or strain gradient [17], dual-scanning technique [18], shifting the Bragg wavelength by the addition of a converging lens before the mask [19].

The Bragg wavelength can be tuned by continuous changing of the grating phase. The phase can be directly controlled by adjusting the relative position of the fiber to the phase mask. Hence chirped profile can be produced by continuously changing the phase [20-21]. Using such moving fiber/phase mask technique, a nonlinear chirped grating with a higher order group delay response can be realized with a complex phase profile. However, producing such a complex phase profile requires a complicated control of the velocity of the fiber mounting platform. Precise controlling of the complex velocity profile of the fiber is not simple. Furthermore the fabrication of nonlinear chirped gratings is difficult hence large errors under this method.

Tuneability in the inscribed Bragg wavelength on a fiber using the phase-mask technique can also be achieved by applying strain to the fiber during the UV exposure stage [21]. The method had been demonstrated in the fabrication of stepped chirped gratings [22]. In this section, we develop a new technique to produce nonlinear continuous chirp grating when the fiber is under a pre-stressing state. Self-apodized continuous nonlinear chirp gratings can then be produced. The ripple of the in-band group delay of less than 10 ps can be achieved.

14

The principal parameters that determine the grating chirp properties are analyzed. Further asymmetric roll-off half-band filtering characteristics of our FBG filters can also be realised.

3.1 Pre-Stretching and grating writing

Figure 7 shows the schematic diagram of the setup used for fabricating the Bragg gratings. The UV beam from a frequency doubled Ar$^+$ laser is folded by a mirror mounted on a motorized translation stage and focused using a cylindrical lens onto the fiber. The UV beam is scanned along the fiber with a velocity controlled by the translation stage motorised platform. The fiber is pre-stretched during the fabrication with one end fixed onto a movable stage and another end clamped by a fixed tower.

The key improvement of our proposed method over previously reported technique [9] is that in our method, the stretched length of the fiber is adjusted during the scanning of the UV beam, and hence continuous chirped grating pitches can be produced, while the technique presented in [22] can fabricate stepped chirp gratings only. To obtain a linear distribution of the in-fiber strain, the fiber coating of the segment between two holders is removed. Because the fiber moves relative to the phase mask during the scanning of the UV, a gradual phase shift is superimposed onto the fiber grating [20]. However, our proposed method is different from the moving fiber/phase mask scanning beam technique [20] in two aspects: firstly, the fiber is stretched and the grating period is chirped during the fabrication process; secondly, the velocity of the fiber is not equal to that of the stage that holds the fiber.
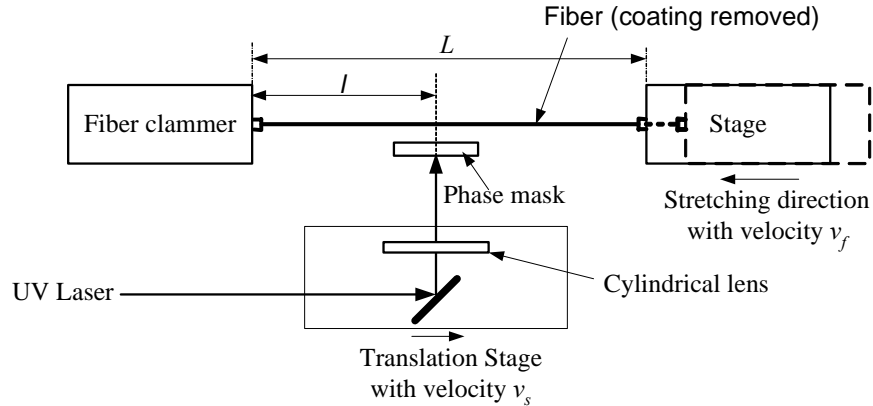
Figure 7 Experimental setup for pre-stretch and writing

If the fiber is moved with a velocity v_f^z, the grating phase shift can be written as

$$\Delta \Phi_f(z) = -\frac{4\pi v_f^z}{\Lambda_p (v_s + v_f^z)} z \qquad (12)$$

15

where Λ_p is the period of the phase mask, v_f^z is the velocity of the fiber at the position of z, v_s is the velocity of the scanning UV beam and $v_s \gg v_f^z$. If the fiber is not stretched (i.e. the two end of the fiber are moving at the same velocity v_f), the method is the moving fiber/phase mask scanning beam technique [20]: the phase shift produced by the moving of fiber produces a change of the centre wavelength given by [10]

$$\lambda = \frac{1}{\dfrac{1}{\lambda_D} - \dfrac{1}{2} \cdot \dfrac{d\Phi_f}{dz}} = (1 + \frac{v_f}{v_s})\lambda_D \tag{13}$$

where $\lambda_D = n_{eff}\Lambda_p$ is the designed wavelength. So the wavelength shift is $\lambda_D v_f/v_s$, as given in [20]. In our method, one end of the fiber is held and the other end of the fiber is moved using a motorized stage. If the velocity of the stage is v_f^0, the velocity of the fiber at position z is given by

$$v_f^z(z) = (l + z) \cdot \frac{v_f^0}{L - \dfrac{v_f^0 z}{v_s}} \approx \frac{v_f^0}{L}(l + z) \tag{14}$$

where l is the distance between the fixed tower and the initial position of the UV beam and L is the length of the fiber between two holders (as shown in **Figure 7**).

In our fabrication system, the fiber is pre-stretched. The stretched length L is adjusted during the UV beam exposure. As a result, the grating period is chirped. The phase distribution of the chirped period is[23]

$$\Delta\Phi_{chirp}(z) = -\frac{4\pi v_f^0 z^2}{\Lambda_p (v_s L + v_f^0 z)} \tag{15}$$

Thus the grating spatial distribution and its center period and can be obtained from (15) as [23]

$$\frac{d\lambda}{dz} = -\frac{\lambda_D^2}{8\pi n_{eff} z} \cdot \frac{d\Phi}{dz} = -\frac{\lambda_D^2}{8\pi n_{eff} z} \cdot \left(\frac{d\Phi_{chirp}}{dz} + \frac{d\Phi_f}{dz} \right) = \frac{\lambda_D v_f^0}{2L v_s}\left(\frac{l}{z} + 4 \right) \tag{16}$$

and

$$\lambda(z) = \begin{cases} \lambda_0 & z = 0 \\ \lambda_0 + \dfrac{\lambda_D v_f^0}{2L v_s}\left(4z + l \cdot \ln(z)\right) & 0 < z < L_g \end{cases} \tag{17}$$

16

where L_g is the length of the grating and λ_0 is the Bragg wavelength at the starting position (z = 0) of the grating. The value of λ_0 is determined by the strain of the grating. It is found that the grating chirp profile consists of a linear factor and a nonlinear factor.

As shown in (1)–(2), larger wavelength shift can be obtained by a faster travelling velocity of the fiber. However, the index modulation is averaged when the fiber moves quicker than the time required for the interference pattern formed onto the fibre by the mask. The index modulation can be given as [20].

$$\delta n = \frac{\sin(2\pi D v_f^z / \Lambda_p v_s)}{2\pi D v_f^z / \Lambda_p v_s} \tag{18}$$

where D is the 1/e diameter of the UV Gaussian beam. In our system, the index modulation decreases with the increasing of v_f^z along the fiber. Thus the fabricated grating is semi-apodized, that is only one end of the grating is apodized. The index modulation vanishes when $v_f^z > \dfrac{\Lambda_p v_s}{2D}$.

3.2   Reflectance Spectra and Group Delay

A nonlinear chirp grating has been fabricated using the above described method. The parameters for the fabrication of the grating are: v_s = 0.01 mm/s, v_f = 0.01 μm/s, L = 185 mm, l = 28 mm and Λ_p = 1070 nm. The grating is inscribed in a Ge:doped silica fiber (PMS-50 from Stockyale Inc.). The group delay is measured using an Agilent optical dispersion analyzer 86038A. **Figure 8** shows the theoretical and experimental reflectance spectra. The 3-dB bandwidth of 1.2 nm is obtained. The two curves agree well, and some differences between the measured and the theoretical spectrum might be caused by fabrication error. Because the weak index modulation might be produced at the starting position of the grating, and the other end of the grating is apodized, thus an asymmetric apodized profile has been formed. **Figure 9** shows the measured and theoretical group delay responses. The measured group delay agrees very well with the theoretical calculated values, and that confirms the prediction given by (6). The linear and quadratic coefficients of the group delay are 215.8ps/nm and 73.6 ps/nm^2, respectively. **Figure 10** also shows the ripples of the group delay. It is observed that the ripples of the in-band group delay are well reduced due to the apodized index modulation. The lowest peak-to-peak ripple of the in-band group delay is less than 10 ps.

A sharp roll off on the right hand side of the filter reflectance spectrum is also observed with more than 25 dB over 0.1 nm while about 1.0 nm on the other side of the reflectance spectrum.
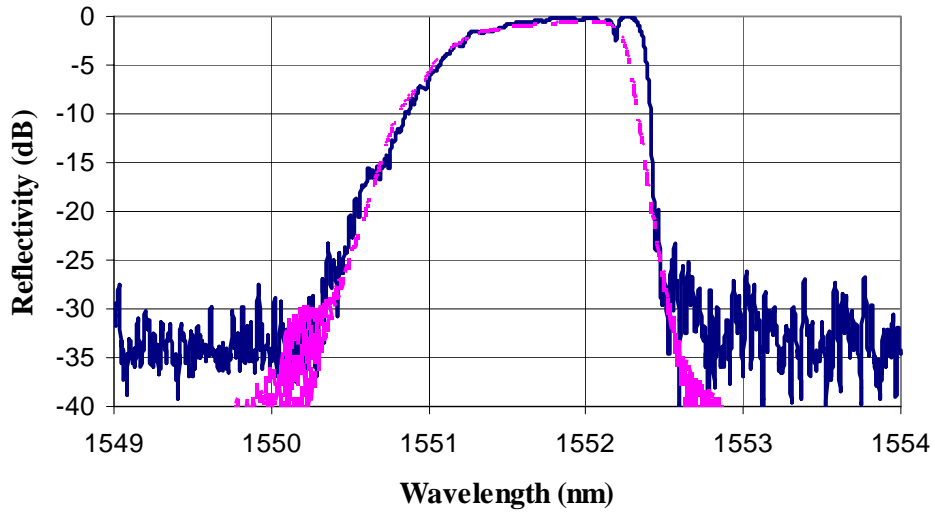
Figure 8 Measured reflective spectrum (solid blue line) and theoretical reflective spectrum

(dashed pink line).

◇ Measured Group delay —— Theoretical group delay
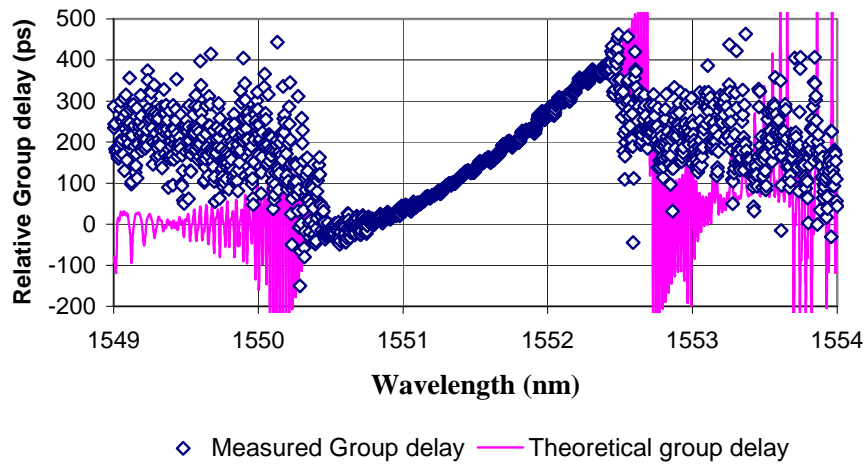
Figure 9 Measured group delay response (markers) and theoretical reflective spectrum (solid pink

line).
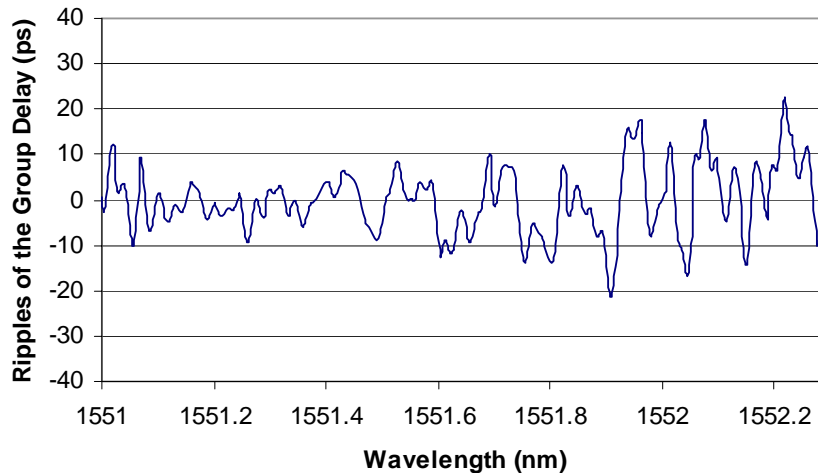
Figure 10 In-band group delay ripples.

3.3 Remarks

IN this section, a new method for fabrication of nonlinear chirped FBGs using a uniform phase mask is presented. The fiber is pre-stretched with the stretched length controlled by a motorized stage while the UV beam scans along the fiber. Asymmetric chirped gratings with nonlinear group delay response are fabricated to demonstrate the novel methodology. The ripples of the group delay can be significantly reduced due to the self-apodized index modulation. Experimental results show a good agreement with those obtained by theoretical prediction. The method enables a simplified fabrication technique for generation of complex chirp profiles. The half-band filtering property of the pre-stretched fibre FBG can be used as a VSB filter for advanced modulation format in long-haul optical transmission systems.

4 INDEX MODULATION PROFILE RECONSTRUCTION BY COMPLEX REFLECTANCE SPECTRA

*This section proposes a new and simple method for reconstruction of the refractive-index modulation of a symmetric FBG from its reflectance spectrum, i.e. the phase information is not needed. The reconstruction method uses an FBG model based on some known FBG parameters including grating length, the number of sub-gratings, and grating period. The Quasi-Newton optimization technique is developed to identify the local parameters of the FBG. The reconstruction of FBG is experimentally realized, **for the first time to the best of our knowledge** by this optimization technique. Comparing with other reconstruction methods, our proposed method is much simpler as requires only the reflectance spectra of the fabricated FBG for optimization.*

Fiber Bragg gratings (FBGs) have been widely used as the key components in wavelength division multiplexed (WDM) systems. Targeting at different applications, many FBGs have

19

been proposed and fabricated by varying the local grating modulation depths of refractive index [25]. In some applications, it is important to understand the discrepancy between the performance of the designed device and the actual device, or study the relationship between index modulation depth and corresponding fabrication conditions (such as the exposure velocity) in order to control the index modulation more precisely. In these applications, it becomes critical to retrieve in-situ the longitudinal index distribution of a grating from its measured complex reflectance spectrum, which includes the reflectivity magnitude and the phase response. This problem is often referred to as the reconstruction problem.

In general, the magnitude of the reflectance does not completely characterize the grating. Both phases and amplitudes must be used. A reflectance spectrum can resemble many possible grating profiles of different phase profiles. Thus all existing methods for reconstructing a grating structure employ both its reflectivity magnitude and phase responses. One of these methods employs the differential inverse scattering algorithm that has been developed for the synthesis of FBGs from their desired complex spectra [26-27]. The other groups use the Gel'Fand-Levitan-Marchenko (GLM) method for finding an iterative solution of the GLM coupled equations [30-31]. Usually measurement of the phase response is not so popular as those using the magnitude reflectance spectrum, hence the reconstruction of gratings is difficult in practice.

The index modulation profile can be determined uniquely from its reflectivity magnitude if the grating is symmetric [32]. Therefore, a symmetric grating can be reconstructed from its reflectivity magnitude, i.e. phase information is not needed. In this section, we employ an optimization algorithm, namely, the Quasi-Newton method, to reconstruct the local grating profiles of a symmetric grating fusing only its measured magnitude reflectance spectrum . That means information of the phase response is not required. As the reconstruction process takes into account the parameters used in the fabrication of the FBG, the reconstructed grating profile can directly identify the relationship between the index modulation depth and the corresponding fabrication conditions (such as exposure velocity, etc.). The proposed method is simple and fast for in-situ direct measurement of the grating's reflectance spectrum. In order to demonstrate the capability of our proposed method, two FBGs are fabricated under the pre-defined symmetrical exposure velocity profile of the translation stage. The scanned phase mask interferometer techniques [33-34], and their profiles are reconstructed.

4.1   Reconstruction algorithm

Fiber gratings can be fabricated by exposing an optical fiber under a spatially varying pattern of an UV beam. The effective refractive index distribution along the longitudinal *z* direction of the fiber after radiation can be assumed as

$$n_{eff}(z) = n_0 + \delta n_{eff}(z) + dn(z)\cos\left[\frac{2\pi}{\Lambda}z + \phi(z)\right] \qquad (19)$$

where n_0 is the effective index of the fiber core before radiation, $\delta n_{eff}(z)$ is the "DC" index change spatially averaged over a grating period, and $dn(z)$ is the profile of the refractive index modulation indicating the "ac" index change. Λ is the nominal grating period and $\phi(z)$ describes the chirp of the grating along the *z* direction. When a grating is fabricated using a uniform phase mask (i.e. no chirp), (19) can simplified as

$$n_{eff}(z) = \overline{n_{eff}}(z) + dn(z)\cos\frac{2\pi}{\Lambda}z \qquad (20)$$

where $\overline{n_{eff}}(z) = n_0 + \delta n_{eff}(z)$ is the profile of the average effective index. It is obvious that the index distribution of the grating includes both the average effective-index profile and the index-modulation profile.

Gratings produced by these techniques (with uniform phase masks) can be assumed to exhibit an index modulation profile of the uniform FBGs exposed under a uniform scanned velocity. Non-uniform FBGs can be produced by stepping a set of continuous velocities, that is generating of a number of uniform FBGs in cascade. Under these conditions, the well-known transfer matrix method (TMM) can be used to model and analyze the complex reflectance spectrum of the FBG [25]. In TMM, each uniform section of the non-uniform FBG can be represented by an analytical transfer matrix. The transfer matrix for the entire grating structure can therefore be obtained by simply multiplying the individual transfer matrices of the uniform gratings. Thus the TMM technique can be used to determine the complex reflectance spectrum of a non-uniform FBG when the index distribution (i.e. $\overline{n_{eff}}(z)$ and $dn(z)$) is given.

The principal objective of the reconstruction problem of the FBG is to find an index distribution (i.e. solution) that produces a reflectance spectrum as close as possible to the measured reflectance spectrum of the FBG. The error between the reflectance spectrum of a given solution and the measured reflectance spectrum is used as one of the criteria. Thus, the objective function to be minimized is given by

$$\text{Error} = \sum_{\lambda} W^{\lambda} \times \sqrt{\left| R^{\lambda}[dn(z), \overline{n_{eff}}(z)] - R^{\lambda}_{\text{measured}} \right|} \qquad (21)$$

where R^{λ} is the calculated reflectivity at a given wavelength λ with an index-modulation profile $dn(z)$ and an average effective-index profile $\overline{n_{eff}}(z)$, $R^{\lambda}_{\text{measured}}$ denotes the measured

reflectivity at a given wavelength λ from the reflectance spectrum, and W^λ is the weight parameter at a particular wavelength. Thus, the reconstruction problem can be formulated as a typical optimization problem, which is to find the minimum of the objective function given in (3). In the optimization procedure, we employ the BFGS Quasi-Newton method with a mixed quadratic and cubic line search procedure, in which the BFGS formula is used for updating the approximation of the Hessian matrix. Detailed description of the algorithm can be found in reference [35].

4.2   Reconstructed profile

The proposed method is verified by reconstructing the index profiles of two FBGs fabricated under pre-defined exposure velocity profiles of the translation stage. To produce a symmetric grating, the exposure velocity is defined with a symmetric profile along the grating length. The relationships between the exposure velocity and the index modulation depth have been found based on the reconstructed results.

4.2.1 Apodized FBG in Ge:doped photosensitive silica fiber

The first grating is written onto a Ge:doped photosensitive silica fiber (PS-RMS-50 from Stockeryale) using a frequency-double Ar$^+$ laser of 50 mW beam power by a scanned phase mask interferometer technique. The length of grating is 10 mm and the period of the phase mask is 1054 nm. **Figure 11** shows an exposure velocity profile for fabricating a self-chirped apodized grating. The grating has 40 sections. Each section produced with different fiber moving velocity value and is treated as a uniform FBG. Therefore, the 10-mm grating consists of 40 piecewise uniform FBGs.
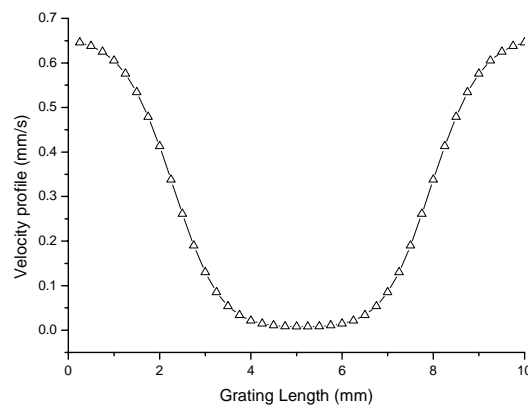
Figure 11 Velocity profile of the translation stage used for the fabrication of the FBG (Ge-doped fiber).

Figure 12 shows the measured reflectivity spectrum of the FBG fabricated using the velocity profile given in **Figure 11**. When each measured reflectivity value of the reflectance spectrum is inserted into (3), the index-modulation profile and the average effective index profile of the FBG can be reconstructed using the proposed method described above. Here we only care about the index-modulation distribution, and the reconstructed index-modulation profile of the grating is given in **Figure 13**. The profile has 40 sections. It can be observed that the slower the exposure velocity, the higher the amplitude of the index modulation. The largest amplitude of the index modulation of 2×10^{-4} corresponds to the slowest exposure velocity of 0.01 mm/s. The modulation ripples on both ends of the grating are probably caused by some kinds of errors in the controlling the translating velocity. The calculated spectrum from the reconstructed index distribution is also given in **Figure 13** for comparison. It is found that the spectrum of the reconstructed grating agrees well with the measured spectrum. The main difference between two spectra is caused by the noise floor level of the spectrum measurement.

Figure 12 Measured reflectance spectrum (solid line) of the fabricated FBG (Ge-doped fiber) and the reconstructed reflectance spectrum calculated numerically using the extracted parameter values of the grating structure (dashed line).

Figure 13 Reconstructed index modulation profile (Ge-doped fiber).

Figure 14 shows the index modulation depth as a function of the velocity of the translation stage. The fitted solid curve has the form as

$$\delta n(v) = 0.03813 + 0.17668 \cdot \exp(-v / 0.08609) \tag{22}$$

where ($\delta n(v)$ is the index modulation depth produced by the exposure velocity v.
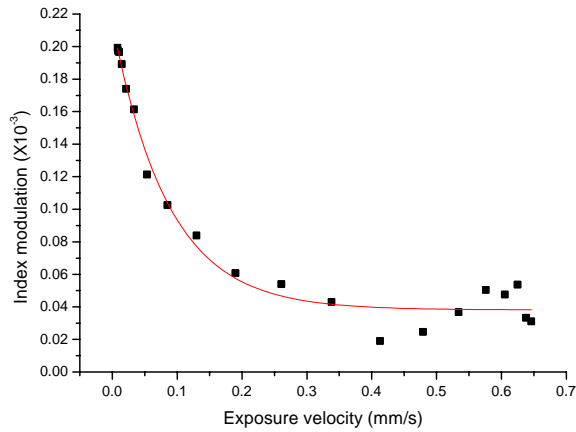
Figure 14 Index modulation depth versus velocity of the translation stage for Ge:doped fiber.

4.2.2 Apodized FBG in B:doped photosensitive silica fiber

The second grating was fabricated in a Boron-doped photosensitive fiber (from Fibercore company). The power of the UV laser is 90 mW. The length of grating was 20 mm and the period of the phase mask was 1070 nm.

24

Figure 15 shows the velocity profile for fabrication of the grating. It can be seen that the grating has 19 sections with a symmetric form. The measured reflectance spectrum of the grating is shown in **Figure 16**. An index modulation profile can be reconstructed as given in its spatial distribution. It is also found that the slower the exposure velocity the higher the amplitude of the index modulation. The calculated reflectance spectrum from the reconstructed index modulation profile is also shown in **Figure 17** as a comparison. The same conclusion is obtained as given in **Figure 12**. The two spectra agree well in those wavelengths that have comparable high reflectivities. **Figure 18** shows the index modulation depth as a function of the velocity of the translation stage for the B-doped fiber under this system (with UV power of 90 mW and 1070 nm phase mask).
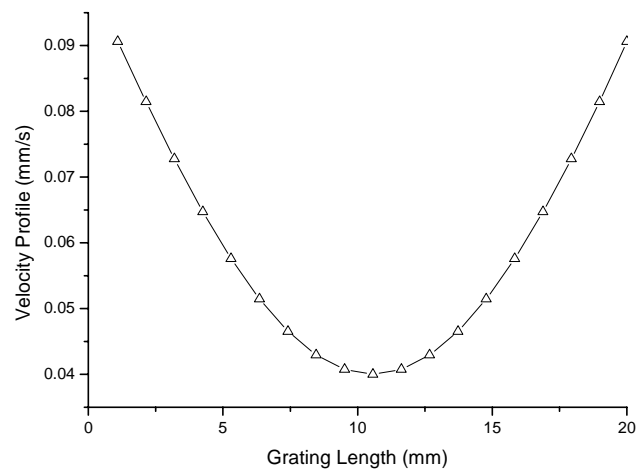
Figure 15 Velocity profile of the translation stage used for the fabrication of the FBG (B-doped
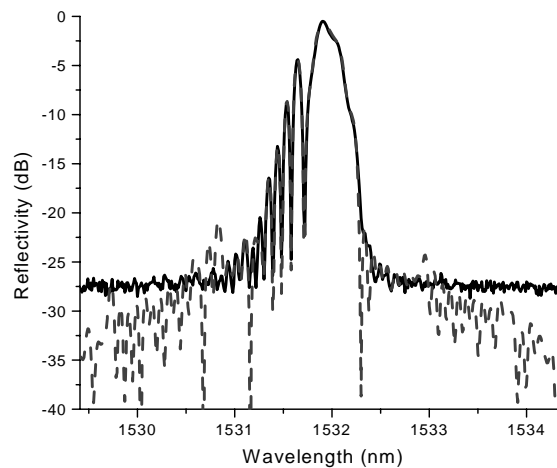
fiber).
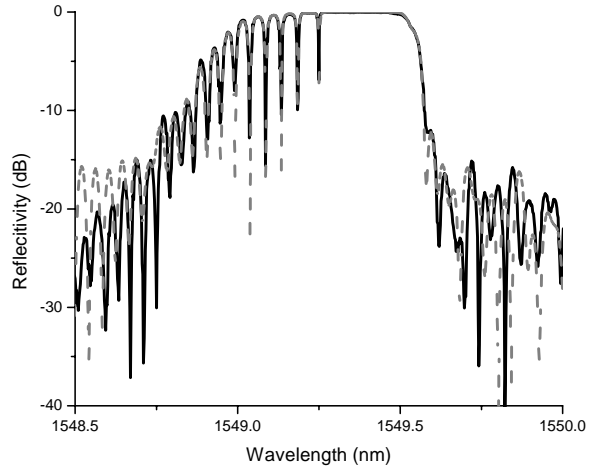
Figure 16

Measured reflectance spectrum (solid line) of the fabricated FBG (B-doped fiber) and the reconstructed reflectance spectrum calculated numerically using the extracted parameter values of the grating structure (dashed line).
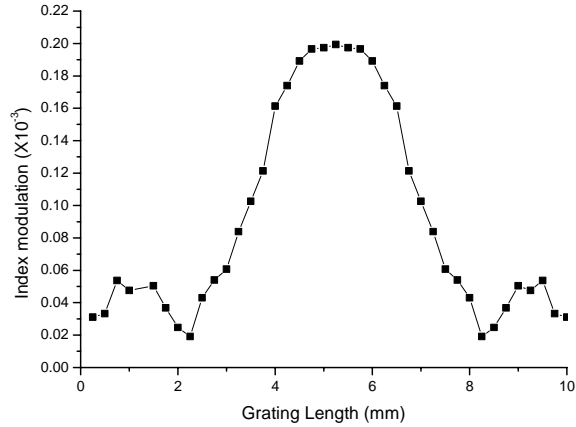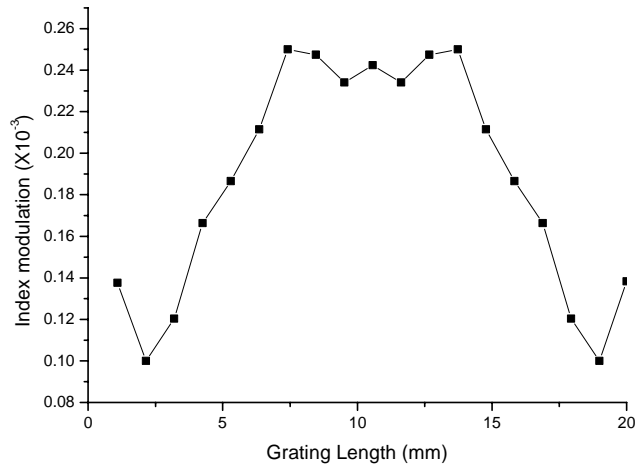

Figure 17 Reconstructed index modulation profile (B-doped fiber).
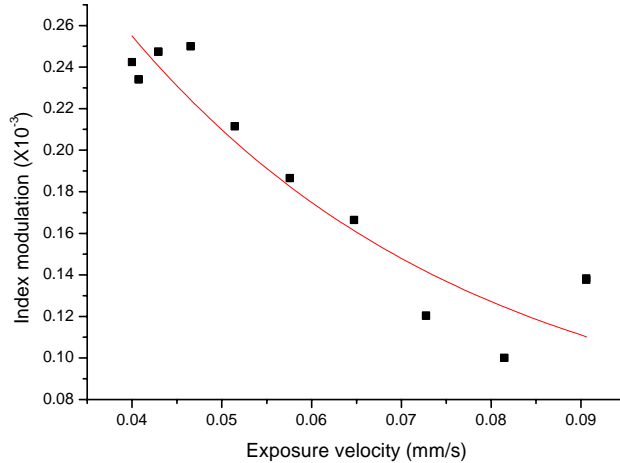
Figure 18 Index modulation depth vs velocity of the translation stage for Boron:doped fiber.

4.3   Remarks

This section has proposed and implemented a new Quasi-Newton optimization algorithm to reconstruct symmetrical FBGs. The proposed method is simple and practical that only the amplitude of the reflectance spectrum is required for reconstruction. The index modulation profiles of two FBGs fabricated with a uniform phase mask have been reconstructed. It is noted that the method is potentially practical for reconstruction of symmetrical FBGs fabricated using scanning interferometer techniques. With this method, it is easy to find the photosensitivity of the fiber (relationship between the exposure velocity and the index modulation depth), hence enabling precisely fabrication of FBGs with complex index modulation. Our proposed method could also be useful in the fabrication of FBGs for telecommunications and sensor network applications.

5   OPTIMIZATION AND FBG SYNTHESES FOR IN-SITU FABRICATION

Sections 2-4 have proposed the novel method for producing gratings with apodized chirp. In practice it is desirable to monitor in-situ the FBG property and synthesize the gratings such that its group delay and reflectance spectra would satisfy certain properties.

In this section, a novel staged continuous Tabu search (SCTS) algorithm is proposed for solving global optimization problems of multi-minima functions with multi-variables. The proposed method comprises three stages that are based on the continuous Tabu search (CTS) algorithm with different neighbor-search strategies, with each devoting to one task. The method searches for the global optimum thoroughly and efficiently over the space of solutions compared to a single process of CTS. The effectiveness of the proposed SCTS algorithm is evaluated using a set of benchmark multimodal functions whose global and local minima are

known. The numerical test results obtained indicate that the proposed method is more efficient than an improved genetic algorithm published previously. The method is also applied to the optimization of fiber grating design for optical communication systems. Compared with two other well-known algorithms, namely, genetic algorithm (GA) and simulated annealing (SA), the proposed method performs better in the optimization of the fiber grating design.

Optimization design is a scientific branch using both scientific methods and technological approaches to satisfy technical, economical and social requirements in an ideal way. Usually, optimization problems in engineering can be formulated as nonlinear programming problems. Due to the multi-modal and ill-condition character of the objective functions, it is difficult to solve these engineering problems with traditional methods. Hence the study of global optimization methods has become one of the most important topics for engineering designers [36].

Tabu Search (TS) is an iterative search method originally developed by Glover [35], which has been successfully applied to a variety of combinatorial global optimization problems [36-38]. A rudimentary form of this algorithm may be roughly summarized as follows. It starts from an initial solution *s* that is randomly selected. From this current solution *s*, a set of neighbours, called *s'*, is generated by pre-defining such a set of 'moves', or perturbation of current solution (see details in Section 5.1). To avoid an endless reiterative cycle, the neighbourhood of the current solution, which belongs to a subsequently defined 'tabu list', is systematically eliminated. The objective function to be minimized is then evaluated for each generated solution *s'*, and the best neighbourhood of *s* becomes the new current solution even if it is worse than *s*. The 'move' that generates the new selected current solution will also be stored in the 'Tabu list', which is circular. When it is full, it is updated by eliminating the previous estimated solution. Then a new 'iteration' is performed: the previous procedure is repeated by starting from the new current point until satisfying stopping condition. Usually, the algorithm stops after a given number of iterations has occurred without any improvement on the value of the objective function.

The more general form of the method uses more advanced recency and frequency memory than embodied in the simple Tabu list, together with associated intensification and diversification strategies that exploit these memory structures (Glover and Laguna [35]). However, simpler forms of TS are sometimes used for conducting prototype studies, and in some instances such methods perform remarkably well without resorting to more powerful forms of TS.

Comparing with analytical methods, even simple versions of the TS algorithm have a smaller probability of becoming trapped in a local optimum. The method is also organized to take advantage of problem-specific information, in contrast to the classical forms of some other

methods such as genetic algorithm (GA) and simulated annealing (SA) approaches[2]. Because of this focus, the method demonstrates a highly attractive convergence velocity as well as a high level of reliability.

Tabu search also includes *candidate list strategies* for generating and sampling neighbourhood. These strategies are extremely important, since often only a relatively small subset of neighbours is generated at any given iteration, especially when large neighbours are used, as in the case of multi-variable problems whose neighbours are generated in a multi-dimensional space. Siarry and Berthiau have proposed a Continuous Tabu Search (CTS) approach [39] for nonlinear function optimization that employs a special candidate list strategy to generate neighbours. In this method, the solution space is divided into several regions. Neighbours are generated in these regions and the remainder of the method consists of an elementary form of TS that uses only the simple Tabu list construction previously mentioned. The authors report impressive results for optimising functions of two or three variables. But when the number of variables increases, the efficiency of the CTS algorithm is not satisfactory and it must be improved for those problems with high dimension [39].

In this section, a new multi-level candidate list method is introduced to give a more effective approach for nonlinear function optimization called Staged Continuous Tabu search (SCTS) algorithm. The algorithm comprises three stages that are based on CTS. Each stage focuses on one task with a special neighbourhood definition, and the combined stages are for global optimization. Section 5.1 gives a brief review on the CTS algorithm. Section 5.2 describes the SCTS algorithm. Section 5.3 presents experimental results of a set of benchmark functions. In Section 5.4, to demonstrate the effectiveness of the proposed method, it is applied to the design of fiber grating, which is an important component in optical communication systems. Conclusions are given in Section 5.5.

5.1   A brief review of the continuous Tabu search algorithm

For the following optimization problem:

$$\min_{s \in \Psi^k}[\Phi(s)], \tag{23}$$

where $\Phi(s)$ is the objective function to be minimized, and $s = [x_1, x_2, \cdots, x_k]^T$ is defined as

$$s \in \Psi^k \text{ and } \Psi^k = \{s \mid a_i \leq x_i \leq b_i\}, i = 1, 2, \ldots, k. \tag{24}$$

---

[2] In recent years, "hybrid variants" of GA and SA methods have emerged that seek to incorporate problem-specific information in a better manner than the classical versions. Some of the more effective instances of these hybrid approaches make use of TS strategies.

a_i and b_i are the boundary values. The basic process of the CTS method, which is organized around a simple version of Tabu search can be summarized as follows:

i.   Generate a random point s that belongs to the space Ψ^k as the current solution.

ii. A set of neighbors $s' \in \Psi^k$ is then generated by applying s with a series of perturbations or 'moves'. Generation of neighbors are defined by the following method: the neighborhood space Ψ^k of the current solution s is deemed as a ball $B(s, r)$ centered on s with a radius r. Considering a set of concentric balls with radii h_0, h_1, ..., h_n, the space is partitioned into n concentric 'crowns'. Hence n neighbors of s are obtained by selecting one point randomly inside each crown and eliminating those neighbors that belong to the 'Tabu list'.

iii. Evaluate these neighbors with the objective function, choose the best neighbor $s*$ and replace the starting point s even if it is worse than the current solution. Then update the 'tabu list'.

iv. Clear the 'Tabu list': in particular, some solutions belonging to the 'tabu list' can release its Tabu status if its 'aspiration level' is sufficiently high.

v.   Check the stopping condition and return to step (ii) if the condition is not met. Otherwise, stop the iteration procedure and report the results.

Figure 19 shows the flow chart of this algorithm, where the main stages include initial solution, generation of neighbors, selection of the solution and Tabu list clearance. From the results reported in [39], the strategy of generating neighbors in CTS is more efficient than a naïve candidate list strategy based solely on random sampling, and usually produces neighbors distributed over the whole solution space[3]. However, the method generally encounters difficulties in finding global optima for high-dimension problems.

---

[3] Other ways of applying tabu search to continuous nonlinear optimization are described in [1], but were not tested in [5].
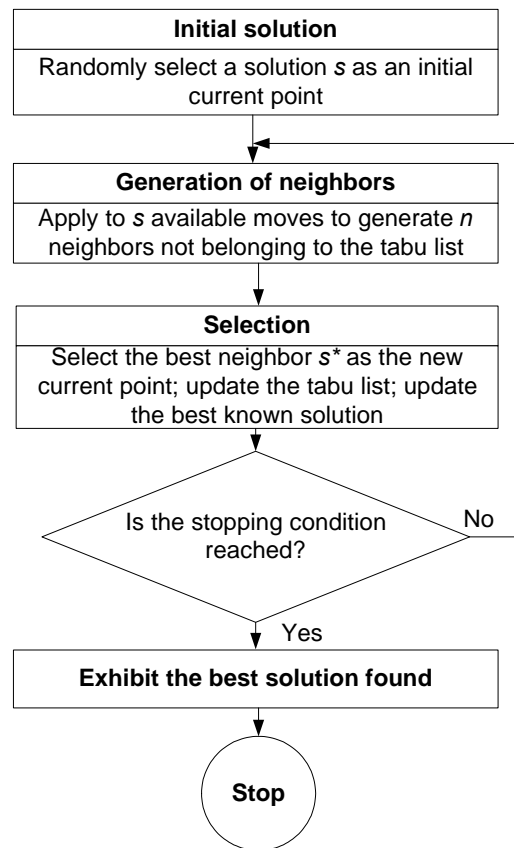
Figure 19 General flow chart of a standard TS algorithm.

5.2 Staged Continuous Tabu Search algorithm

A new Staged Continuous Tabu Search (SCTS) algorithm is developed to improve on the CTS algorithm. The SCTS algorithm likewise employs the same rudimentary form of Tabu search embodies in CTS, but provides an enhanced candidate list strategy that subdivides the CTS approach into three independent processes that generate candidate neighbors in different ways. The first stage tries to survey the whole solution space to localize a 'prospective point', which is a solution likely to produce a global optimum. The objective of the second stage is to find a point close to the global optimum. The third stage starts from the solution found in the second stage, and eventually converges to the global optimum point. The proposed SCTS algorithm is described below.

● *Generation of neighborhoods*

As described in the CTS method in Section 5.2, the neighborhoods are generated in a ball $B(s,r)$ centered on *s* with radius *r*. All neighbors s' meet the condition: $|s'-s| \leq r$.

In the first stage, the radius r_1 is defined so that the sphere $B_1(s,r_1)$ contains the whole k-dimension space Ψ^k. With radii $r_1^1, r_1^2, \cdots, r_1^{n_1}$, the ball is partitioned into k concentric 'crowns' centered on the current solution. One neighbor is produced in each crown. Thus the ith neighbor s_i' is generated with the condition:

$$r_1^{i-1} \le |s_i'-s| \le r_1^i, \ (r_1^0 = 0). \tag{25}$$

As the ball $B_1(s,r_1)$ includes the whole space Ψ^k, it should be possible for all solutions within it to become the neighbors of the current solution s so that the process can investigate the whole solution space. We define the 'moves' to generate neighbors such that some elements of the current solution are randomly replaced. The number of replaced elements depends on different crowns. For example, the ith neighbor s_i' is generated by replacing any i elements of the current solution.

The radius r_2 for the generation of neighbors in the second stage is defined as the minimum radius of radii $r_1^1, r_1^2, \cdots, r_1^{n_1}$. Followed with another partition process with a set of radii $r_2^1, r_2^2, \cdots, r_2^{n_2}$, the sphere $B_2(s,r_2)$ is divided into n_2 sections. The ith neighbor s_i' is generated with a condition given by

$$r_2^{i-1} \le |s_i'-s| \le r_2^i, \ (r_2^0 = 0). \tag{26}$$

As described above, the minimum radius defined in the first stage is propagated in only one dimension of the current solution. Considering the condition defined in (2), we can proportionally divide the boundary for every dimension into n_2 partitions. The neighbors can then be generated by replacing the ith element of the current solution (x_i') with a number computed by:

$$x_i' = a_i + (j+\mu) \cdot \frac{(b_i - a_i)}{n_2} \cdot \text{ where } i=1, 2, ..., k; \ j=1, 2, ..., n_2. \tag{27}$$

where k is the dimension number of the current solution s, and μ is a random value between 0 and 1. It can be seen that the number of neighbors in this stage is $k \times n_2$.

The minimum of radii $r_2^1, r_2^2, \cdots, r_2^{n_2}$ is set as the radius r_3 to generate neighbors in the third stage. Instead of partitioning to generate neighbors, the radius of the ball $B_3(s,r_3)$ decreases with an increase in the iteration number. The generation of the ith neighbor is defined as

$$x_i' = x_i + \mu_i \cdot \frac{b_i - a_i}{n_2} \cdot (\frac{M_3 - m}{M_3})$$

(28)

where x_i and x_i' are the ith elements of the current solution *s* and the neighbor s' produced, respectively, *μ* is a random value between -1 and 1, *m* is the iteration number without any improvement on the current solutions, and M_3 is the maximum allowable number of iterations without any improvement.

- *Tabu list*

In the underlying TS algorithm, a Tabu list stores some solutions that have recently been selected. It is used to qualify the algorithm to select solutions that have not been selected before so as to escape from being recycled.

Because the three stages in the SCTS algorithm are independent each other, the tabu lists in these stages are thus independent. The list obtained in the first stage will store those 'prospective solutions' found in recent iterations. In the second and third stages, the list will store the attributes of 'moves' or perturbations that generate the best neighbors in recent iterations. The tabu list in each stage is always reset at the beginning of each stage.

- *Stopping conditions*

The stopping conditions for the three processes are defined as:

i. The program will stop after a given number of iterations without any improvement on the value of the objective function. The number of iterations differs in different stages.

ii. The results satisfy the successful conditions. This stopping condition only applies to problems with known global optima (such as the benchmark test functions as presented here).

iii. The search procedure will stop after a pre-defined maximum number of iterations.

In the SCTS algorithm, in the first stage, if any one of the stopping conditions is reached then the program will move to the second stage. This also applies to the second stage. In the last stage, the program will stop if any one of the stopping conditions is reached.

- *Description of the Algorithm*

*Figure 20*shows a flowchart of the steps of the proposed SCTS algorithm.
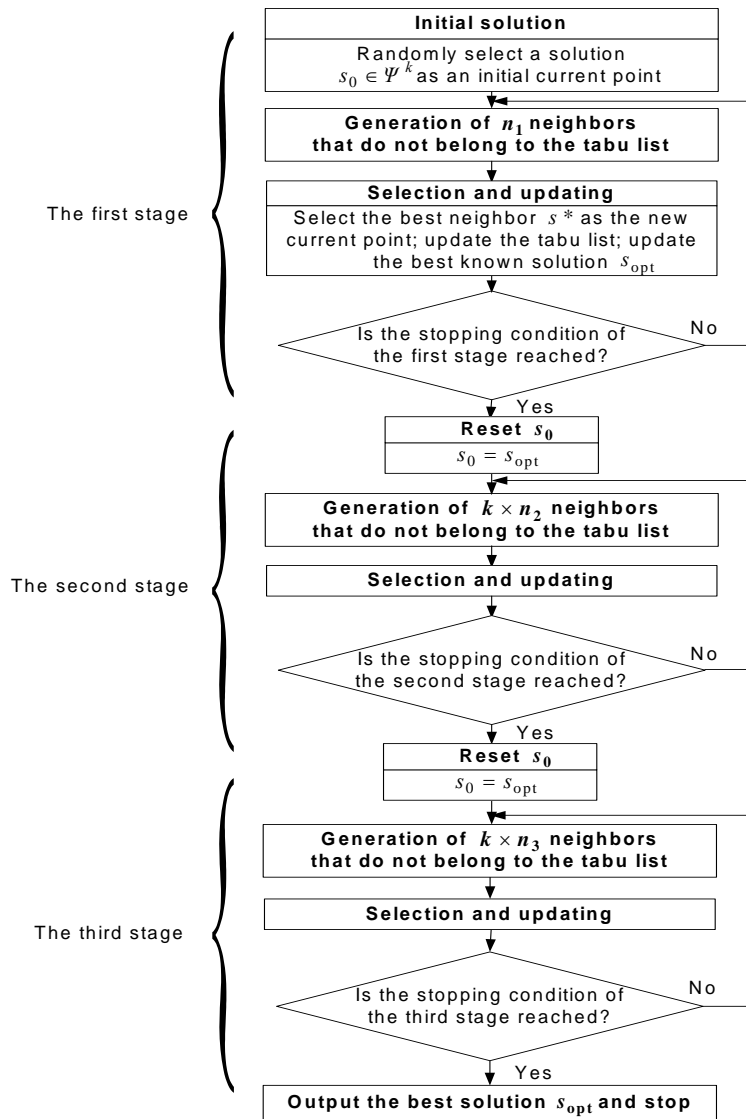
Figure 20 Algorithmic description of the proposed SCTS algorithm.

The following notations are used: Ψ^k: Space of feasible solutions (*k* dimensions); s_0: Current solution; n_1:Length of neighbors generated in the first stage, which is equal to *k* here; n_2: The section number divided within the boundary of every element of s_0. n_3: Length of neighbors generated in the third stage; s': The neighborhood of s_0; he best solution in s'; s_{opt}:Current best solution found; *Mv(i)*:maximum number of iterations without improvement of s_{opt} in the ith stage.

As pointed out previously, the neighbors in the first stage are generated in the largest range so as to explore most of the space. While in the last stage, only a reduced space is used so that the solution finally converges to the global optimum.

The sensitivity some main parameters in the CTS algorithm has already been discussed in detail in [39]. Usually, these parameters should be adjusted empirically according to different problems in order to achieve an efficient optimisation process. As inherited from the CTS algorithm, it is found that some parameters in the SCTS algorithm have similar properties as those of the CTS algorithm. However, we have not analysed in detail the variation of the parameters and have only applied a set of empirical values of the parameters in our experiments of the benchmark functions to test the effectiveness of the SCTS algorithm.

5.3   Numerical Tests

To demonstrate the effectiveness of the algorithm, the important parameters to be studied are convergence, speed and robustness. The test for convergence employed here is the relative error between the optimum obtained by the algorithm, X_{opt}, and a theoretical value of the optimum, X_{theo}, of each function. The relative error, E_{relative}, can be defined as [40]

$$E_{\mathrm{relative}} = \frac{\left| X_{\mathrm{opt}} - X_{\mathrm{theo}} \right|}{X_{\mathrm{theo}}} \tag{29}$$

If the theoretical value of the optimum is zero, the relative error in equation (29) becomes

$$E_{\mathrm{relative}} = \left| X_{\mathrm{opt}} - X_{\mathrm{theo}} \right| \tag{30}$$

The criterion of speed means the time taken by the algorithm to find the global optimum of the objective function. However, the computation time also depends on the computation speed of the computer. Thus, we define the speed criterion by determining the number of evaluations of the objective function required till a global optimum is found.

Robustness means that the algorithm is versatile and can be applied to solving a variety of functions. A set of commonly used benchmark test functions whose global optima are known, and listed in the Appendix, is chosen to test our algorithm. These test functions represent various practical problems in science and engineering. To obtain a statistical comparison of the optimization results, every test has been performed 100 times (starting from various randomly selected points) to ensure that the results obtained are reliable.

Table 1 shows the results obtained from the proposed SCTS algorithm for the four test functions, namely, Goldprice, Hartmann34, Branin and Shubert. The criterion of success is the percentage of trials (out of the 100 tests for each function) that can reach the global optimum with a relative error of less than 1%. Experimental data obtained from the CTS

algorithm [29] is also shown in the table. From the table, it can be seen that both the algorithms can successfully find the global optima of all the four test functions. Compared with the CTS algorithm, the SCTS algorithm reduces the number of evaluations of the Goldprice test function from 1636 to 696 and the Shubert test function from 1123 to 521. This means that the SCTS algorithm has a faster computation rate for these two particular functions. However, for the Hartmann34 and Branin functions, the SCTS algorithm does not show much improvement over the CTS algorithm, showing that the algorithms are equally fine for these two particular functions.

Table 1 Experimental data of the SCTS and CTS algorithms.

Function	Successful rate (%)		Number of evaluation functions	
	CTS	SCTS	CTS	SCTS
Goldprice	100	100	1636	696
Hartmann34	100	100	528	691
Branin	100	100	668	491
Shubert	100	100	1123	521

Table 2 shows a comparison of the experimental data of various test functions obtained by the SCTS algorithm with an improved genetic algorithm (IGA). It is noted that the IGA algorithm can potentially yield a complete set of optima when dealing with multimodal problems [30]. These test functions have variables from 1 to 20 as given in the Appendix. In the table, the minimum found (Max) is the maximum value of the optimum found and the minimum found (Min) is the value of the minimum of optimum found over 100 tests.

From **Table 2**, the SCTS algorithm outperforms the IGA algorithm in two ways. One advantage is that the SCTS algorithm can find the global optima (see, for example, the Brown1, Brown 3 and F10n functions) that the IGA algorithm fails to find.

Table 2. *Experimental data of the test functions obtained by the proposed SCTS algorithm and the improved Genetic Algorithm (IGA).*

Function	Number of variables	Theoretical minimum	Minimum found (Min)		Minimum found (Max)		Relative error average (%)		Number of evaluation of test functions		Success rate (%)	
			IGA	SCTS	IGA	SCTS	IGA	SCTS	IGA	SCTS	IGA	SCTS
F1	1	-1.1232	-1.1232	-1.1232	-1.1139	-1.1223	0.03	0	784	134	100	100
F3	1	-12.0312	-12.0312	-12.0312	-11.9270	-12.0203	0.12	0	744	181	100	100
Branin	2	0.3979	0.3979	0.3979	0.4018	0.3983	0.48	0	2040	492	100	100
Goldprice	2	3	3.003	3.002	3.0296	3.0029	0.43	0	4632	696	100	100
Shubert1	2	-186.7309	-186.6857	-186.7304	-184.9554	-186.3406	0.53	0.014	8853	2194	100	100
Shubert2	2	-186.7309	-186.7047	-186.7302	-184.9295	-185.9505	0.53	0.024	4116	2053	100	100
Shubert	2	-186.7309	-186.7280	-186.7269	-184.8753	-186.5490	0.49	0.0003	2364	521	100	100
Hartmann3	3	-3.8628	-3.8611	-3.8621	-3.8246	-3.8591	0.51	0.018	1680	560	100	100

4											
Brown1	20	2	8.5516	2.0018	111.2914	2.0020	2692.67	0.05	128644	111430	0	100
Brown3	20	0	0.6746	0.0006	5.9122	0.0010	2.324	0.0009	106859	15142	5	100
F5n	20	0	0.0022	0.0001	0.5906	0.0010	0.067	0.0004	99945	17443	100	100
F10n	20	0	0.0496	0.0001	4.0660	0.0010	1.197	0.0008	113929	19931	49	100
F15n	20	0	0.0034	0.0003	0.7361	0.0009	0.075	0.0008	102413	19660	100	100

In these cases, the SCTS algorithm can successfully find the global optima for those functions that the IGA algorithm cannot obtain a successful rate of 100%. Moreover, the relative errors obtained by the SCTS algorithm for these functions can reach a satisfactory level of close to zero. The other advantage is that the SCTS algorithm greatly reduces the computation time as indicated by the smaller number of evaluation of the test functions. In addition, the SCTS algorithm reduces the relative error for those functions for which the global optima obtained by the IGA algorithm with a successful rate of 100%. These test functions are F1, F3, Branin, Goldprice, Shubert1, Shubert2, Shubert, Hartmann34, F5n and F15n.

5.4   Application of the SCTS algorithm to the syntheses of FBGs

The increasing demand for high transmission capacity requires the channel spacing of dense wavelength division multiplexing (DWDM) channels to be very narrower and narrower (e.g. 50 GHz and less). It is therefore important to develop optical filters with block-wall like spectral response that can separate wavelength channels of such narrow channel spacing with minimum crosstalk. FBG technology can meet this required performance. FBG can be produced by exposing a photosensitive fiber to a spatially varying pattern of ultraviolet intensity. They have several unique advantages which include small size, low loss, low polarization sensitivity, all-fiber geometry, easy fabrication, and low cost. A uniform FBG is the simplest type of FBG in design and fabrication but the roll-off between the passband and the cut-off band of its reflection spectrum is not sharp due to the presence of the secondary maxima on both sides of the main reflectance peak. This is due to the finite length of the uniform FBG with a constant modulation depth of the refractive index along the fiber length. Therefore non-uniform FBGs with square-like spectra are required for the DWDM application.

The transfer matrix method (TMM) is normally used to obtain the spectra of non-uniform FBGs [42]. In TMM, the non-uniform FBGs are divided into a number of serially-connected uniform sub-gratings or sections.
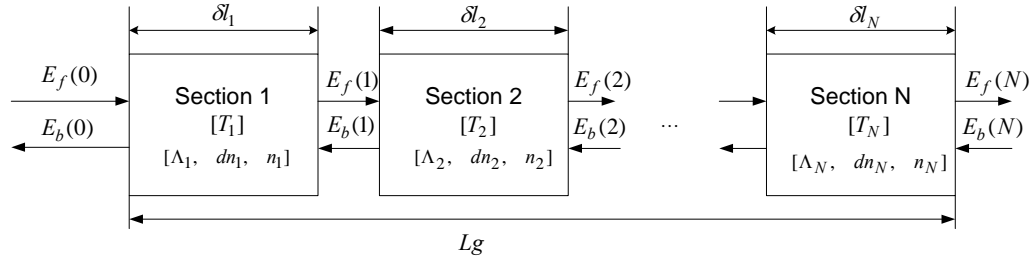
Figure 21 Schematic diagram of the piecewise-uniform FBG.

Every uniform section has an analytic transfer matrix. The transfer matrix for the entire structure can be obtained by multiplying the individual transfer matrices. In Figure 21, $E_f(i)$ and $E_b(i)$ are complex electric fields of the forward and backward propagation waves, respectively, describing the ith section. δl_i, Λ_i, dn_i and n_i are the length, grating period, amplitude of index modulation and average effective index of the ith section, respectively. *Lg* is the length of whole grating. The electric fields at the input and output ports of the FBG are given by

$$\begin{bmatrix} E_f(0) \\ E_b(0) \end{bmatrix} = T_1 \cdot T_2 \cdots T_N \begin{bmatrix} E_f(N) \\ E_b(N) \end{bmatrix} \tag{31}$$

where T_i is the transfer matrix of the ith section of the FBG.

Applying the boundary condition, $E_b(N) = 0$ (i.e. there is no input to the right side of the FBG), the reflection R, which is a function of wavelength, is given by

$$R = \left| \frac{E_b(0)}{E_f(0)} \right|^2 \tag{32}$$

Thus, the problem of optimizing the FBG with a target spectrum can be defined as

$$\min \left(\sum_{\lambda \in \text{window}} W_\lambda \left| R_\lambda(dn, n, \Lambda, \delta l) - R_{\lambda, \text{target}} \right| \right) \tag{33}$$

where W_λ is the weight parameter used to adjust the requirements in different wavelength λ range over the optimization wavelength window. $R_{\lambda, \text{target}}$ and $R_\lambda(dn, n, \Lambda, \delta l)$ are the target reflectivity and calculated reflectivity with specified grating parameters at the wavelength λ.

The Genetic algorithm (GA) and Simulated Annealing algorithm (SA) have been applied to solve such problems of optimization of FBGs [41-42]. In this section, as an example to demonstrate the effectiveness of the proposed SCTS algorithm to solving an important engineering problem, it is applied to the design of an FBG with an optimized block-wall like spectral response. Hence, the target spectrum is defined as

$$R_{\lambda, \text{target}} = \begin{cases} 1 & 1549.9 \quad \text{nm} \quad \leq \quad \lambda \quad \leq \quad 1550.1 \quad \text{nm} \\ 0 & \lambda \quad < \quad 1549.9 \quad \text{nm} \quad \text{and} \quad \lambda \quad > \quad 1550.1 \quad \text{nm} \end{cases} \quad (34)$$

Because only the index modulation profile is optimized here, the other parameters of the grating (i.e. grating period, average effective index and grating length) are pre-specified. The reflectance at a particular wavelength λ is a function of the index modulation profile, which can be described by the transfer matrix method. The index modulation profile is thus expressed by $dn = [dn_1, dn_2, \cdots, dn_N]^{\text{T}}$ with the condition

$$dn_{ia} \leq dn_i \leq dn_{ib}, \quad (i = 1, 2, \ldots, N) \quad (35)$$

where N is the number of sections, dn_{ia} and dn_{ib} are the boundaries set for the ith element of dn.

In this design, the number of sections is chosen as $N = 40$, and the boundary of dn is set as $[0, \quad 0.0002]$, and the parameters of the SCTS algorithm are listed in *Table 3*.

Table 3 Typical parameter values of the SCTS algorithm used for both the benchmark test functions and the optimized design of the FBG.

List of parameters for SCTS algorithm	Parameters used for benchmark functions	Parameters used for optimization of FBG
Number of neighbors in the first stage (n_1)	Number of variables	40
Number of sections in the second stage (n_2)	5	5
Number of neighbors in the third stage (n_3)	Number of variables	40
Number of neighbors in the second stage	5×Number of variables	5×40=200
Maximum number of iterations without any improvement on the objective function value (Mv)	{40, 10, 10}	{40, 10, 10}
Maximum number of iterations of SCTS algorithm	8000	8000

Figure 22 shows the optimized index modulation profile of a 1-cm long FBG as optimized by the SCTS algorithm. The corresponding spectral response is illustrated in **Figure 23**. It can be seen that the spectrum of the uniform FBG (without optimization) has the undesirable secondary maxima or sidelobes of up to ~ 30% on both sides of the main reflection peak. The

39

sidelobes could create crosstalk or interference in the DWDM application. These sidelobes are greatly suppressed by the optimized FBG designed by the SCTS algorithm.
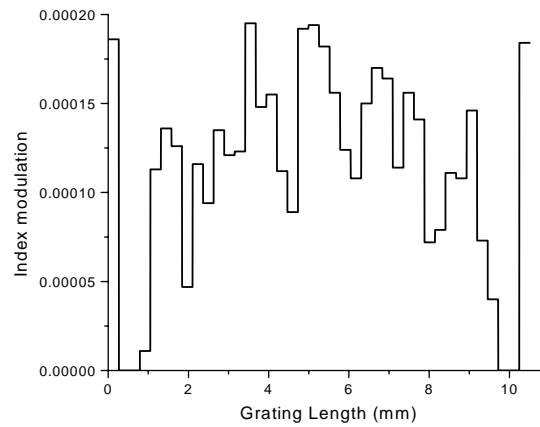

Figure 22 *Optimized index modulation profile of the designed FBG using the SCTS algorithm.*
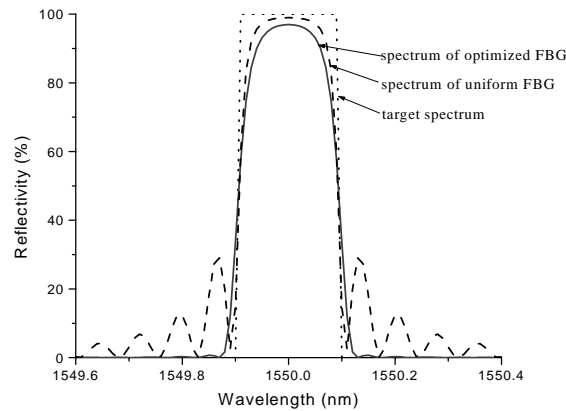

Figure 23 Spectral response of the optimized FBG design using the SCTS algorithm. Solid line is the spectral response of the optimized FBG; Dotted line is the desired spectrum (target spectrum); *Dashed line is the spectral response of the uniform FBG (non-optimized).*

To verify that the optimum solution of the FBG design obtained by the SCTS algorithm is indeed the global one, two other algorithms, namely, the GA and Adaptive SA (ASA) algorithm presented in references [44-46] are employed here for comparison. Table 4 shows the optimum of the objective function (as given in (11)) obtained by the three algorithms. It is clear that the SCTS algorithm provides the best result with the smallest optimum value.

Table 4. The minimum value of the objective function obtained by the three algorithms.

Algorithm applied	GA	ASA	SCTS
Minimum found	4.9583	5.3451	4.9370

It is to be noted that we have directly used the algorithms from references [54-55] but the softwares did not give the exact number of evaluations of the objective function. To compare the computation speed, the three software programs were run on the same computer, and it was found that the GA algorithm had the longest computation time while the computation time of the ASA algorithm is similar to that of the SCTS algorithm.

5.5   Remarks

We have proposed an effective global optimization algorithm, namely, the SCTS algorithm by combining three stages of the CTS algorithm with three strategies of neighborhood generation. From the test results of a number of benchmark test functions, it has been found that the SCTS algorithm is more effective than the original CTS and the IGA in terms of the success rate and computation efficiency. It has also been shown that the SCTS algorithm is a powerful tool for solving some engineering problems such as the optimization of the FBG design. Future research works would focus on incorporating more advanced forms of the underlying Tabu search approach to obtain additional improvements in performance.

Acknowledgement

6   REFERENCES

[1] F. Quellette, "All-fiber filter for efficient dispersion compensation," Opt. Lett. vol. 16, no. 5, pp. 303−305, 1991.

[2] J. A. R. Williams, I. Bennion, and L. Zhang, "In-fiber pulse compression using linearly chirped Bragg-gratings," in CLEO/Europe-EQEC 1994 postdeadline papers, Amsterdam, pp. 26−27.

[3] J. Azana and M. A. Muriel, "Temporal self-imaging effects: Theory and application for multiplying pulse repetition rates," IEEE J. of Selected topics in Quan. Electron., vol. 7, no. 4, pp. 728−744, 2001.

[4] K. O. Hill, F. Bilodeau, B. Malo, T. Kitagawa, S. Theriault, D. C. Johnson, J. Albert, and K. Takiguchi, "Chirped in-fiber Bragg gratings for compensation of optical-fiber dispersion," Opt. Lett., vol. 19, no. 17, pp. 1314−1316, 1994.

[5] J. D. Prohaska, "Magnification of mask fabricated fiber Bragg gratings," Electron. Lett., vol. 29, pp.1614−1616, 1993.

[6] M. J. Cole, W. H. Loh, R. I. Laming, M. N. Zervas and S. Barcelos, "Moving fibre/phase mask-scanning beam technique for enhanced flexibility in producing fiber gratings with uniform phase mask," Electron. Lett., vol. 31, no. 17, pp. 1488−1450, 1995.

[7] Asseh, "A writing technique for long fiber Bragg gratings with complex reflectivity profiles," J. of Lightwave Tech., vol. 15, pp. 1419−1423, 1997.

[8] Petermann, B. Sahlgren, S. Helmfrid, A. T. Friberg, and P. Y. Fonjallaz, "Fabrication of advanced fiber Bragg gratings by use of sequential writing with a continuous-wave ultraviolet laser source," Appl. Optics., vol. 41, no. 6, pp. 1051−1056, 2002.

[9] R. Kashyap, "Design of step-chirped fibre Bragg gratings," Opt. Commun., vol. 136, pp. 461−469, 1997.

[10] R. Kashyap, P. F. McKee, R. J. Campbell, and D. L. Williams, "Novel method of producing all fibre photoinduced chirped gratings," Electron. Lett., vol. 30, no. 12, pp. 996−998, 1994.

[11] K. C. Byron and H. N. Rourke, "Fabrication of chirped fibre gratings by novel stretch and write technique," Electron. Lett., vol. 31, no. 1, pp. 60-61, 1995.

[12] G. Imeshev, I. Hartl, and M. E. Fermann, "Chirped pulse amplification with a nonlinearly chirped fiber Bragg grating matched to the Treacy compressor," Opt. Lett. vol. 29, no. 7, pp. 679−681, 2004.

[13] Z. Xiong, G. D. Peng, B. Wu, and P. L. Chu, "Highly tunable Bragg gratings in single-mode polymer optical fibers," IEEE Photon. Technol. Lett., vol. 11, pp. 352−354, 1999.

[14] J. Lee, S. Kim, Y. Kim, Y. Oh, S. Hwang, J. Jeong "Optically pre-amplified receiver performance due to VSB filtering for 40 Gb/s optical signals modulated with various formats", IEEE J. Lightw. Tech., Dec. 2003.

[15] T. Inui, T. Komukai, M. Nakazawa, K. Suzuki, K. R. Tamura, K. Uchiyama, T. Morioka, "Adaptive dispersion slope equalizer using a nonlinearly chirped fiber Bragg grating pair with a novel dispersion detection technique," IEEE Photonics Technology Lett., vol. 14, no. 4, pp. 549−551, April, 2002.

[16] K. M. Feng, V. Grubsky, D. S. Starodubov, J. X. Cai, A. E. Willner and J. Feinberg, "Tunable nonlinearly-chirped fiber Bragg grating for use as a dispersion compensator with a voltage-controlled dispersion," OFC 1998, TuM3, pp. 72−74.

[17] J. Kwon, Y. Jeong, S. Chung, and B. Lee, "Tailored chirped fiber Bragg gratings using tapered elastic plates," OFC 2002, Thgg43, pp. 672−673.

[18] J. A. R. Williams, L. A. Everall, L. Bennion and N. J. Doran, "Fiber Bragg grating fabrication for dispersion slope compensation," IEEE Photonics Technology Lett., vol. 8, no. 9, pp. 1187−1189, 1996.

[19] J. D. Prohaska, "Magnification of mask fabricated fiber Bragg gratings," Electron. Lett., vol. 29, pp. 1614−1616, 1993.

[20] Asseh, "A writing technique for long fiber Bragg gratings with complex reflectivity profiles," J. of Lightwave Tech., vol. 15, pp. 1419−1423, 1997.

[21] M. J. Cole, W. H. Loh, R. I. Laming, M. N. Zervas and S. Barcelos, "Moving fibre/phase mask-scanning beam technique for enhanced flexibility in producing fiber gratings with uniform phase mask," Electron. Lett., vol. 31, no. 17, pp. 1488−1450, 1995.

[22] Q. Zhang, "Tuning Bragg wavelength by writing gratings on prestrained fibers," IEEE Photonics Technology Lett., vol. 6, pp. 839−841, 1994.

[23] K. C. Byron and H. N. Rourke, "Fabrication of chirped fibre gratings by novel stretch and write technique," Electron. Lett., vol. 31, no. 1, pp. 60−61, 1995.

[24] T. Erdogan, "Fiber grating spectra," IEEE J. Lightwave Technol., vol. 15, pp. 1277−1294, 1997.

[25] T. Erdogan, "Fiber grating spectra," IEEE J. Lightwave Technol., vol. 15, pp. 1277−1294, 1997.

[26] R. Feced, M. N. Zervas, and M. A. Muriel, "An efficient inverse scattering algorithm for the design of nonuniform fiber Bragg gratings," IEEE J. Quantum Electron., vol. 35, pp. 1105−1115, 1999.

[27] L. Poladian, "Simple grating synthesis algorithm," Opt. Lett., vol. 25, pp. 787−789, 2000.

[28] J. Skaar, L. Wang, and T. Erdogan, "On the Synthesis of fiber Bragg gratings by layer peeling," IEEE J. Quantum Electron., vol. 37, pp. 165−173, 2001.

[29] P. Giaccari, H. G. Limberger, and R. P. Salathe, "Local coupling-coefficient characterization in fiber Bragg gratings," Opt. Lett., vol. 28, pp 598–600, 2003.

[30] E. Peral, J. Capmany, and J. Martin, "Iterative solution to the Gel'Fand-Levitan-Marchenko coupled equations," IEEE J. Quantum Electron., vol. 32, pp. 2078–2084, Dec. 1996.

[31] S. Keren, A. Rosenthal, and M. Horowitz, "Measuring the structure of highly reflecting fiber Bragg gratings," IEEE Photon. Technol. Lett., vol. 15, pp. 575–577, Apr. 2003.

[32] L. Poladian, "Group-delay reconstruction for fiber Bragg gratings in reflectance and transmission", Opt. Lett., vol. 22, no. 20, pp. 1571–1573, Oct. 1997.

[33] J. Martin and F. Ouellette, "Novel writing technique of long and highly reflective in-fibre gratings," Electron. Lett., vol. 30, pp. 811–812, 1994.

[34] H. N. Rourke, S. R. Baker, K. C. Byron, R. S. Baulcomb, S. M. Ojha and S. Clements, "Fabrication and characterisation of long, narrowband fibre gratings by phase mask scanning", Electron. Lett., vol. 30, pp. 1341–1342, 1994.

[35] D. F. Shanno, "Conditioning of Quasi-Newton Methods for Function Minimization," Mathematics of Computing, vol. 24, pp. 647–656, 1970.

[36] F. Glover, M. Laguna, Tabu Search, Kluwer Academic Press Pub., 1998.

[37] J. M. Machado, S. Yang, S. L. Ho and P. Ni, "A common Tabu search algorithm for the global optimization of engineering problems," Comput. Methods Appl. Mech. Engrg., vol. 190, pp. 3501-3510, 2001.

[38] D. Karaboga, D. H. Horrocks, N. Karaboga and A. Kalinli, "Designing Digital FIR Filters Using Tabu Search Algorithm," IEEE International Symposium on Circuits and Systems, Hong Kong, June 9-12, 1997, pp. 2236-2239.

[39] S. L. Ho, S. Y. Yang, G. Z. Ni, H. C. Wong, "An improved Tabu Search for the Global Optimizations of Electromagnetic Devices", IEEE Transactions on Magnetics, vol. 37, pp. 3570-3574, 2001.

[40] P. Siarry, G. Berthiau, "Fitting of tabu Search to optimize functions of continuous variables", International J. for Numerical Methods in Engineering, vol. 40, pp. 2449-2457, 1997.

[41] J. Andre, P. Siarry, T. Dognon, "An improvement of the standard genetic algorithm fighting premature convergence in continuous optimization," Advances in engineering software, vol. 32, pp. 49-60, 2001.

[42] J. Skaar, K. M. Risvik, "A Genetic Algorithm for the Inverse problem in Synthesis of Fiber Gratings," IEEE J. of Lightwave Technol., vol. 16, no. 10, pp. 1928-1932, 1998.

[43] J. Bae, J. Chun, "Design of Fiber Bragg Gratings Using the Simulated Annealing Technique for an Ideal WDM Filter Bank," IEEE MILCOM 2000. 21st Century Military Communications Conference Proceedings, 2000, vol. 2, pp. 892 –896.

[44] T. Erdogan, "Fiber Grating Spectra," IEEE J. of Lightwave Technol., vol. 15, no. 8, pp. 1277-1294, 1997.

[45] C. Houck, J. Joines, and M. Kay, "A Genetic Algorithm for Function Optimization: A Matlab Implementation," NCSU-IE TR 95-09, 1995. http://www.ie.ncsu.edu/mirage/GAToolBox/gaot/.

[46] L. Ingber, "Adaptive simulated annealing (ASA): Lessons learned," Control and Cybernetics, vol. 25, pp.33-54, 1996. http://www.ingber.com.

[47] R. T. Zheng, N. Q. Ngo, P. Shum, S. C. Tjin, and **L. N. Binh,** "A staged continuous Tabu search algorithm for the global optimization and its applications to the design of fiber Bragg gratings", Computational Optimization and Applications, vol. 30, 2004, pp. 117.

[48] R. T. Zheng, N. Q. Ngo, **L. N. Binh,** and S. C. Tjin, "Two-stage hybrid optimization of fiber Bragg gratings for design of linear phase filters", Journal of Optical Society of America A, vol. 21, 2004, pp. 2399-2405.

[49] R. T. Zheng, N. Q. Ngo, **L. N. Binh**, S. C. Tjin, and J. L. Yang, "Nonlinear group delay using asymmetric chirped gratings written in fibers under pre-stretched conditions", Optics Communications, vol. 242, 2004, pp. 259-265.

[50] R. T. Zheng, N. Q. Ngo[*], **L.N. Binh**, S. C. Tjin, and P. Shum "An Optimisation Technique for Simple Reconstruction of the Index Modulation Profile of Symmetric Fiber Bragg Gratings from their Reflective Spectrum" IEEE Journal of Lightwaves Technology, in Press, 2004.

7   APPENDIX: List of Test Functions

- F1 (1 variable):

$$f(x) = 2(x - 0.75)^2 + \sin(5\pi x - 0.4\pi) - 0.125 \text{ where } 0 \le x \le 1$$

- F3 (1 variable):

$$f(x) = -\sum_{i=1}^{5}\{i\sin[(i+1)x + i]\} \text{ where } -10 \le x \le 10$$

- Branin (2 variables):

$$f(x, y) = a(y - bx^2 + cx - d)^2 + h(1 - g)\cos(x) + h$$

where $a = 1, b = \dfrac{5.1}{4\pi^2}, c = \dfrac{5}{\pi}, d = 6, h = 10, g = \dfrac{1}{8\pi}$,

- Goldprice (2 variables):

$$f(x, y) = [1 + (x + y + 1)^2(19 - 14x + 3x^2 - 14y + 6xy + 3y^2)]\times$$

$$[30 + (2x - 3y)^2(18 - 32x + 12x^2 + 48y - 36xy + 27y^2)]$$

- Hartmann1 ($H_{3,4}$) (3 variables)

$$f(x) = -\sum_{i=1}^{4} c_i \exp\left[-\sum_{j=1}^{3} a_{ij}(x_j - p_{ij})^2\right] \text{ where } 0 < x_j < 1 \text{ for } j = 1 \sim 3$$

- Shubert1 and 2 (2 variables):

$$f(x) = \left\{\sum_{j=1}^{5} j \cdot \cos[(j+1)x + j]\right\} \times \left\{\sum_{j=1}^{5} j \cdot \cos[(j+1)y + j]\right\} +$$

$$+ \beta[(x + 1.42513)^2 + (y + 0.80032)^2]$$

where $-10 \le x, y \le 10$, $\beta = 0.5$ for Shuber1, and $\beta = 1$ for Shuber2.

- Shubert (2 variables):

$$f(x) = \left\{ \sum_{j=1}^{5} j \cdot \cos[(j+1)x_1 + j] \right\} \times \left\{ \sum_{j=1}^{5} j \cdot \cos[(j+1)x_2 + j] \right\} \text{ with } -10 \le x_i \le 10 ,$$

i=1,2;

● Brown1 (20 variables):

$$f(x) = \left[\sum_{i \in J} (x_i - 3) \right]^2 + \sum_{i \in J} [10^{-3}(x_i - 3)^2 - (x_i - x_{i+1}) + e^{20(x_i - x_{i+1})}] \qquad \text{with}$$

$J = \{1, 3, \cdots 19\}$

$-1 \le x_i \le 4$ for $1 \le i \le 20$ and $x = [x_1, \cdots, x_{20}]^T$

● Brown3 (20 variables):

$$f(x) = \sum_{i=1}^{19} \left[(x_i^2)^{(x_{i+1}^2 + 1)} + (x_{i+1}^2)^{(x_i^2 + 1)} \right] \text{ with } x = [x_1, \cdots, x_{20}]^T \text{ and } -1 \le x_i \le 4 \text{ for}$$

$1 \le i \le 20$

● F5n (20 variables):

$$f(x) = (\pi / 20) \times \left\{ 10 \sin^2(\pi y_1) + \sum [(y_i - 1)^2 \times (1 + 10 \sin^2(\pi y_{i+1}))] + (y_{20} - 1)^2 \right\}$$

where $x = [x_1, \cdots, x_{20}]^T$, $-10 \le x_i \le 10$ and $y_i = 1 + 0.25(x_i - 1)$

● F10n (20 variables):

$$f(x) = \left(\frac{\pi}{20} \right) \times \left\{ 10 \sin^2(\pi x_1) + \sum_{i=1}^{19} \left[(x_i - 1)^2 \times (1 + 10 \sin^2(\pi x_{i+1})) \right] + (x_{20} - 1)^2 \right\}$$

where $x = [x_1, x_2, \cdots x_{20}]^T$ and $-10 \le x_i \le 10$

● F15n (20 variables):

$$f(x) = (1/10)\{ \sin^2(3\pi x_1) +$$

$$\sum_{i=1}^{19} [(x_i - 1)^2 (1 + \sin^2(3\pi x_{i+1}))] + (1/10)(x_{20} - 1)^2 [1 + \sin^2(2\pi x_{20})] \}$$

where $x = [x_1, x_2, \cdots x_{20}]^T$ and $-10 \le x_i \le 10$.